GIMA
Geographical Information Management and Applications

Greening measures to mitigate urban heat islands during tropical nights in Vienna, Austria

Marina Lanxinger
marina.lanxinger@gmail.com

Professor: dr.ir. Lammert Koistra (WUR)
Supervisor: dr.ir. Ron van Lammeren (WUR)

Acknowledgements

This thesis was written within the scope of the Master's program "Geographical Information Management and Applications" (GIMA).

I would like to thank my supervisor dr.ir. Ron van Lammeren for his time to supervise and support me during the whole process and for being very encouraging and motivating along the way. Further, I want to thank dr.ir. Lammert Koistra, the responsible professor for this thesis, who gave some very useful inputs especially in the beginning stage.

I would like to thank my dear friend Julia Gastegger, with whom I spent weekends working together, for her support, the delicious breakfasts and her positive attitude.

התודה הכי מיוחדת לרון מודחי, אהבת חיי, שעודד אותי ותמך בי אפילו להתחיל את התזה הזו ולצערי איבדתי אותו בדרך. לא יכולתי לעשות את זה בלעדייך.

Abstract

Population growth and continuing urbanization have become major threats in the ongoing climate crisis, as more than half of the earth's population lives in cities. Floor sealant and densification processes lead to transformations in the urban microclimate. The appearance of the so-called urban heat island (UHI) effect, when temperatures tendentially stay higher within areas of sealed surfaces than around less built-up areas, is increasing. During summer months, when daily temperatures rise above 30°C and simultaneously heat periods occur, another phenomenon is likely to happen. So-called tropical nights are very warm nights, when temperatures stay above 20°C. The link of both phenomena has not been targeted in research yet, as nighttime UHI studies are relatively rare. Accordingly, comparatively little is known about heat mitigation measures to target heat islands during tropical nights. However, increasing the amount of vegetation in urban areas has a significant positive impact on UHI in general. The InVEST urban cooling model is an option to show the influence of green cover in relation to a city's cooling capacity. A heat mitigation index is calculated by use of several parameters, such as land use/land cover, evapotranspiration, building intensity or the distance from cooling islands like parks. Based on that, scenarios can be developed by simply modifying the input land cover map, which sheds light on temperature reduction by vegetation in urban areas.

Table of Contents

1 INTRODUCTION

In the past decades, global climate change has moved increasingly into focus, given the fact that global mean surface temperature has risen since the 20th century. Urbanization contributes to a significantly extent to global warming, considering that more than 50% of the human population lives in cities. Both population growth and urbanization have caused the worldwide observed phenomenon of Urban Heat Islands (UHI) (Kaplan et al., 2018; Zhou et al., 2018).

Urban heat and cool islands are common phenomena in urban areas when temperatures tend to be higher around sealed surfaces than within less built-up areas due to heat storage. It describes the difference in air temperature between high-tempered urban areas and low-tempered rural areas. The causes of this phenomenon are mainly urbanization, structural changes of land surface and industrialization (Tyrallová et al., 2018). The re-use of large brownfield sites as well as densification of the urban structures without additional measures intensify the UHI effect. Both urban residents and tourists are affected by Urban Heat Islands, but especially people who have to spend much time in open space, health-impaired and elderly people suffer from it. Besides minor consequences such as the reduction of activity due to heat, heat waves cause a great number of deaths each year (Czachs et al., 2013).

One suitable option to reduce UHI effects is the preservation and expansion of green spaces. Besides cooling the actual space, they can also influence the surrounding area, which is called the urban green space cooling effect (Aram et al., 2019). Aram et al. (2019; p.26) distinguishes 5 categories to reduce UHI effects: "*(1) the use of vegetation cover like trees, (2) shrubs and lawns at different scales, (3) the stack night ventilation, (4) the use of waterbodies, and (5) the use of materials with high albedo rating for pavement and other ground surfaces".* The effectiveness of green space in mitigating UHI effects is already proven through measurements and computer simulation. A broad variety of literature is available that focuses on different shapes and scales. (Aram et al., 2019).

1.1 PROBLEM STATEMENT

Heat days and heat periods in Vienna and other European cities have increased in the past decades (Czachs et al., 2013). Whereas heat days refer to days with a maximum temperature of at least 30°C, heat periods describe leastwise three consecutive days of temperatures of 30°C or above. For the latter one the mean maximum temperature must reach 30°C over the whole period, but must not fall below 25°C (Kyselý et al., 2000). With the rise of daily maximum temperatures, the occurrence of very warm nights is increasing too. These so called "tropical nights", when temperature stays above 20°C, are impacting people's well-being and mortality more significantly than maximum daily temperatures (Czachs et al., 2013). Figure 1 shows the increase of tropical nights in Vienna over the past decades with a significant rise since the 1990s. While the purple line indicates the

annual number of tropical nights, the black line illustrates the moving average of 30 years.

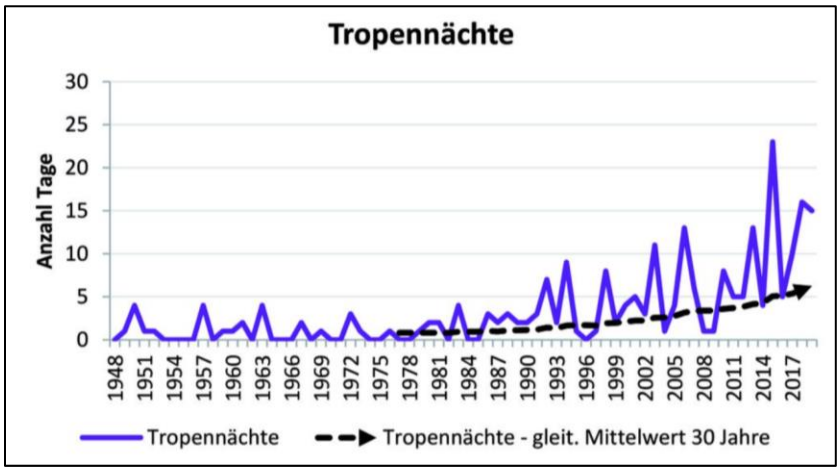

Figure 1: Number of tropical nights in Vienna over the past decades (IBO – Österreichisches Institut für Baubiologie und -ökologie, 2021)

The number of hot days in Vienna during the period of 1961 to 2010 rose from an average of 9,6 to 15,2 days. Simultaneously, some climate models forecast an increase of summer days, when temperature reaches 25°C or more, of 30 to 50 percent for the end of this century which can lead to the rise of the Urban Heat Islands (UHI) effect (Czachs et al., 2013).

Literature on urban climate has shown the significance of nocturnal UHI phenomenon. During the nighttime, the effects of UHI are more apparent, due to lower cooling capacity of urban construction materials. The negative impacts on people's health tend to aggravate especially at night during extreme events such as heat waves. Despite these facts, the study of nocturnal UHIs is still poorly developed, by cause of structural problems such as the availability of land surface and air temperature data for the nighttime (Roca & Arellano, 2020).

1.2 SCIENTIFIC RELEVANCE

In the past few decades, advancements of remote sensing as well as progress of spatial science have significantly increased the number and quality of surface urban heat island (SUHI) studies, which are the centerpiece of urban heat island (UHI) literature. SUHI represents the difference of land surface temperature (LST) in urban relativity to adjacent non-urban surfaces and is usually measured by the use of satellite LST data (Zhou et al., 2018).

The city of Vienna has started taking interest in the issue of urban heat islands more than 20 years ago. Since then, basic studies and active information gathering have been conducted, as well as strategy plans have been developed supported by Vienna's Department of Environmental Protection MA22. The initiatives included preparing climate studies, preparing a climate assessment and climate function map acquired from thermal imaging, and implementing measures such as green

space networks, green roofs, living walls and rainwater management (Czachs et al., 2013).

Even though, the government of Vienna has been proactive to target the problem of heat stress within the city, the above-mentioned initiative dates already back to 2014. Vuckovic et al. (2019) states that unplanned transformation of existing urban areas causes increasingly inhomogeneity in cities, with more impermeable (sealed) than permeable (vegetative) cover. This process is problematic from a climatic and thermal point of view, but also impacts the perception of urban areas as favorable living environment.

Furthermore, the conducted study of the city of Vienna focuses only on in-situ measurements and computer modeling to forecast urban heat islands, but does not include remote sensing data. Arellano and Roca (2021) mention the same lack of remote sensing approaches for nocturnal UHI, as the obtainment of them is primarily following two traditional methods, which is either the extrapolation of data from weather stations, or the calculation of air temperatures trough urban transects.

1.3 RESEARCH AREA

The research area compasses the capital of Austria, Vienna, which is situated in the northeastern corner of Austria, between the foothills of the Alps and the Carpathians (Encyclopædia Britannica, 2021). Alongside the Danube, Europe's second longest river, Vienna covers an area of 41 487ha (Encyclopædia Britannica, 2021 & Magistrat der Stadt Wien, 2021). The altitude of Vienna ranges from its lowest point of 151m to 543m at its highest point.

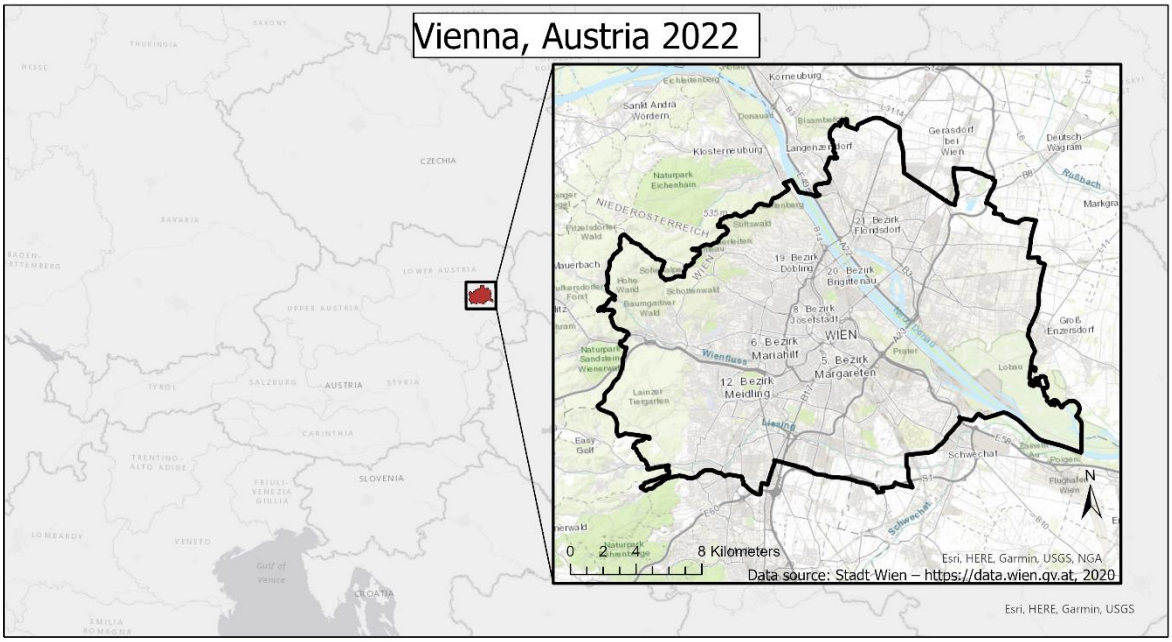

Figure 2: Location of Vienna

Climatological, Vienna is influenced by two climates, which are oceanic from the west and continental from the east. Winters are relatively mild compared to other parts of Austria. This shows in less rainfall and longer dry periods (Magistrat der Stadt Wien, 2021).

Vienna has been rated the city with the highest worldwide quality of living by Mercer a several times in the past years. Its current population comprises 1,92 million inhabitants which is steadily growing (STATISTICS AUSTRIA, 2021 & ISOCARP Institute, 2021). Within the period of the years 2013 till 2017 the Viennese population increased on average by around 30 000 inhabitants per year, causing the annual need for about 10 000 new apartments. Therefore, densification in new settlement areas requires the need of a clear understanding of the current and future microclimatic situation in built-up areas. An analysis of Vienna's land use found, that about half of the city area can be considered green, such as parks, agricultural lands and urban forests. However, the locations of the green areas are not evenly distributed. While inner districts possess 2% to 15% green space, the western districts come with up to 70% green coverage, due to their hilly topography and forested areas (ISOCARP Institute, 2021).

2 THEORETICAL BACKGROUND

2.1 URBAN CONFIGURATIONS AND URBAN MICROCLIMATE

In the past decades, population growth in urban areas has continuously increased. As a result, urban areas are facing high building densities, which, again, impact the urban microclimate (Allegrini et al., 2015). Thereby, urban heat islands have become one of the urban climatology problems. Drastic reduction of green areas to built-up areas is seen as one of the main causes of UHI, whereas trees and vegetation play a vital role for mitigation strategies (Buyadi et al., 2013). Kong et al. (2014) found that in areas with a higher percentage of forest-vegetation a greater cooling effect can be experienced. Moreover, an increase of 10% in forest-vegetation causes a decrease of approximately 0.83°C in surface temperature.

Urban configuration can impact the local thermal environment due to altering energy balances. However, the urban heat island effect can be intensified by both urban sprawling and compact urban development (Yue et al., 2019). Unplanned transformation of existing urban areas leads to increasingly inhomogeneity with more impermeable (sealed) than permeable (vegetative) cover. Not only climatic and thermal issues arise with it, but also the overall perception of urban areas as favorable living environments is becoming challenged. More informed planning strategies are indispensable to allow for environmentally friendly urban development and mitigation of negative phenomena associated with global urbanization. Urban densification has emerged as a promising strategy. Nevertheless, the potential of urban densification to counteract negative implications of urbanization lacks scientific investigation and documentation (Vuckovic et al., 2019).

2.2 URBAN HEAT ISLAND EFFECT

Mesoscale factors are the main determinants of a city's climate. However, local and micro-scale factors, such as topography, different characteristics of the urban structure, surface of roofs, vegetation or anthropogenic heat among others, can impact the regional climate on urban level. Comparing the climate of urban areas to those of a rural nature, there are substantial differences (Arellano & Roca, 2021).

"*The urban heat island effect (UHI) describes the influence of urban surfaces on the temperature patterns of urban areas as opposed to surrounding areas*." (Arellano & Roca, 2021; p.15)

Accordingly, urban heat islands are urban areas that are significantly warmer than its rural surroundings, due to human activities and artificial infrastructures. Opposed to rural areas with high coverage of grass, crops, shrubs or forest, urban areas tend to be dominated by paved grounds. Vegetation contributes to cool the air, whereas asphalt and concrete absorb heat and thus lead to rising temperatures. In addition, narrow streets and buildings trap heat by reducing air flow. Urban

traffic and the heating of buildings also add to the occurrence of UHI (Copernicus Europe's Eyes on Earth, 2022). As indicated in figure 3, vegetation cover absorbs less heat, while using evapotranspiration for cooling. In urban spaces surfaces absorb more heat, but has less cooling from evaporation and plant transpiration due to the lack of vegetation.

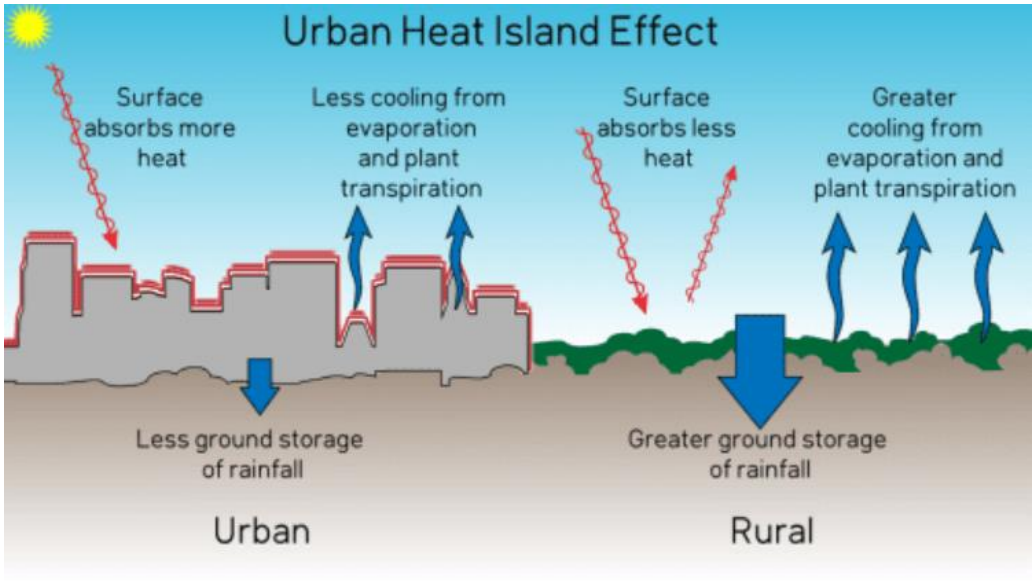

Figure 3: Schematic representation of the urban heat island effect (DOZR Inc., 2021; https://dozr.com/blog/urban-heat-island)

Artificial materials, primarily asphalt and concrete are the main causes of the occurrence of UHI. Due to the greater thermal inertia of the materials used in urban areas, the UHI effect becomes more distinct during the night. At nighttime heat accumulates in urban materials, especially during heat waves, by reason of the low cooling capacity of urban construction materials (Arellano & Roca, 2021). Sobstyl et al. (2018) describe two factors that dominate nighttime UHI. One reason is the ability of materials to store solar radiation during the day, while the other one is the rate at which this energy is released at night. Anthropogenic heat may cause additional energy but does not play a major role during nighttime.

As a result of the microclimate increased by the UHI, the demand for energy to enable the cooling of building increases, which fortifies the generation of power, and moreover, leads to an increased amount of greenhouse gases emission and decline of climate (Nuruzzaman, 2015). According to Akbari et al. (2001) the increase of temperature of 1°C results in the rise of electricity demand of approximately 2-4%. On the other hand, if UHI mitigation measures are taken, 20% of energy used for air conditioning can be saved in order to reduce the UHI effect. (Nuruzzaman, 2015).

Intensive studies to understand the UHI effect have been conducted and lead to the classification of two broad categories, which are "air" or "atmospheric" and "surface" UHIs. While air UHIs relate to UHI effects in the canopy (CLHI) or

boundary (BLHI) layer, surface UHIs (SUHI) represent the radiative temperature difference between urban and non-urban surfaces. SUHIs are mainly derived from satellite thermal remote sensing data and allow for various spatial and temporal scales (Zhou et al., 2018).

2.3 LAND SURFACE TEMPERATURE

"Land Surface Temperature (LST) is the radiative skin temperature of the land derived from infrared radiation" (ESA, 2000-2021). "Skin" temperature relates to the temperature of the top surface when in bare soil conditions, as well as to the effective emitting temperature viewed from the top of a canopy. To put this definition in a rather simplified manner, LST refers to how hot the surface of the Earth would feel to the touch in a designated location. Surface can be various things from a satellite's point of view, such as snow and ice, the grass on a lawn, the roof of a house or the leaves in the canopy of a forest. However, LST cannot be equalized with the air temperature that is shown in daily weather reports (ESA, 2000-2021). Nevertheless, LST is a vital parameter for many fields of interest like surface energy and water balance, climatology, meteorology, ecology, agriculture, environment, and hydrology. In these fields it provides a substantial understanding of a wide range of applications involving surface heat islands and urban climate studies among many others (Sekerteking & Bonafoni, 2020).

Remote sensing analysis for SUHI detection is considered a promising technique which is suitable for large urban areas at a given time. Images are acquired from satellites and aircraft equipped with sensors that capture the short and long wavelength radiation energy reflected from the earth's surface. The essential spectral band for this kind of analysis ranges from 0.1 lm to 100 lm (Bahi et al., 2020). The obtainment of LST of different permeable and impervious materials is a complicated procedure (Bahi et al., 2020; Sekertekin & Bonafoni, 2020). Considering a sparsely vegetated area, the calculated LST will comprise the surface temperature of vegetation and soil combined. LST accuracy is mainly influenced by surface parameters (emissivity and geometry), sensor parameters (spectral range and viewing angle), and atmospheric effects. To obtain LST from Thermal Infrared (TIR) data, accurate estimation of Land Surface Emissivity (LSE) and atmospheric parameters is indispensable (Sekertekin & Bonafoni, 2020).

2.3.1 Indicators of LST

The most common used indicator to describe a surface urban heat island is the difference of urban and rural surface temperatures. However, several other indicators exist and have been used to quantify surface urban heat islands in various studies (Schwarz et al., 2011). For the classical approach, the differentiation between "urban" and "rural" needs to be analyzed which remains a bit of a challenge. The conceptual model of Lowry (1977) defines rural areas as parts of a city region that are not impacted by the urban heat island, which makes the differentiation between urban and rural areas a result of the urban heat island analysis. However, definitions of remote sensing studies are often based on land

cover. A variety of methods are used to delineate the "urban core" versus the "rural part" (Schwarz et al., 2011), such as *"pixels around urban and rural weather stations […]; pixels with high imperviousness versus a buffer lying 15 to 20 km away from low imperviousness areas […]; and areas with the highest LST versus areas with rural land cover"* (Schwarz et al., 2011; p.3176). Moreover, further indicators have been developed, for example the difference of urban versus water, the hot island area, the shape properties of a fitted three-dimensional Gaussian bell and the magnitude of the LST.

2.4 URBAN HEAT ISLAND MITIGATION MEASURES

The phenomenon of UHI exists in almost every big city (Nuruzzaman, 2015). Yamamoto (2006) claims that the elimination of the UHI effect is not feasible, but the key issue is how to best mitigate it (Nuruzzaman, 2015). Numerous works have shown a strong relation between sustainability and climate change based on the interaction of the urban ecosystems and the global climate system. Hence, many sustainable practices have been adopted as solutions to tackle UHI and keep a balanced living environment, while also contributing in temperature mitigation and providing sufficient energy (Sahnoune & Benhassine, 2017). Among various strategies to reduce urban heat, raising the amount of vegetation is considered one of the most effective ways to conquer UHI (Nuruzzaman, 2015).

2.4.1 Green Infrastructure

Greening urban areas comes with a lot of advantages. Vegetation regulates the microclimate through evapotranspiration from plant foliage and shading of the surfaces. In addition, it positively influences human thermal comfort (Balany et al., 2020). The benefits of so-called green infrastructure (GI) for urban microclimates, however, varies by size, location and types of vegetation. Benedict & McMahon (2012; p.1) defines GI as *"an interconnected network of natural areas and other open spaces that conserves natural ecosystem values and functions, sustains clean air and water, and provides a wide array of benefits to people and wildlife."* GI includes both natural and designed greening, including parks and street trees, as well as green roofs, gardens and green laneways (Balany et al., 2020). The urban green infrastructure (UGI) as a multifunctional network provides multiple ecological benefits by providing ecosystem services, but also by contributing to human well-being (Ring et al., 2021).

3 RESEARCH QUESTIONS AND OBJECTIVES

3.1 MAIN OBJECTIVE

The main objective of this thesis is the evaluation of urban greening scenarios for urban heat island mitigation during tropical nights. Thus, this thesis aims to show urban greening scenarios which could help to mitigate extreme heat during nighttime. The focus point will be on the nocturnal heat hot spots of Vienna, which need to be identified and mapped first. For the hotspot area the status quo of the current green share and its heat mitigation potential will be evaluated. Thereafter, generated greening scenarios are supposed to shed light to the mitigation of heat in Vienna. The whole research will be executed in consecutively order, as the research questions are based on each other.

3.2 RESEARCH QUESTIONS

The main research question persists of two minor research questions, which are all listed below. Moreover, research questions 1 and 2 are further divided into sub-questions.

How can different greening scenarios to mitigate urban heat islands during tropical nights in Vienna be evaluated?

- R1: Where are the urban heat islands of tropical nights in Vienna?
    - Which thermal data are most suitable for nighttime UHI detection in Vienna?
    - How can Vienna's detected urban heat islands be validated?
    - How can the temperature hotspots be defined area wise in Vienna?

- R2: How can greening measures to mitigate urban heat islands during tropical nights in Vienna be mapped in different scenarios?
    - What is the current green share in the most significant tropical night's temperature hot spot in Vienna?
    - How sensitive is the change of land cover to land surface temperature in Vienna?

4 METHODOLOGY

4.1 OVERVIEW

The conceptual model in Figure 4 gives an overview of the basic methodological steps. The coloring refers to different research questions that are tackled, which subdivides this research into 2 main execution sections.

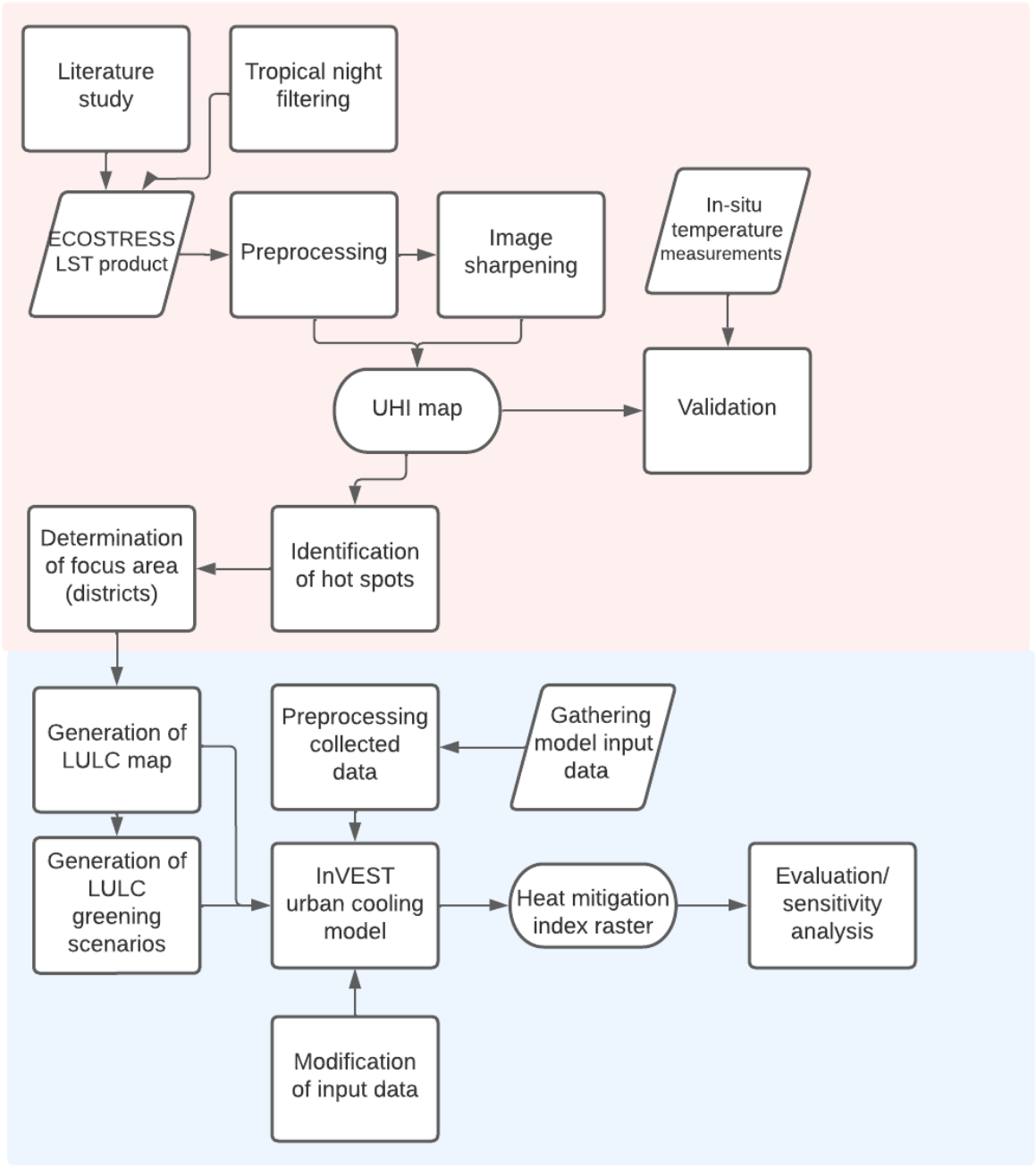

Figure 4: Workflow diagram

To begin with, research question 1, colored in red in the workflow diagram, required intense literature study before focusing on the analysis part. It deals with the calculation of urban heat islands by the use of land surface temperature. Since the use of LST ECOSTRESS data was decided by both literature study and the consultation of an expert, the actual LST calculation is not part of this thesis. Instead, image sharpening was executed to gain higher spatial resolution and thus more detailed information about nighttime UHI. Validating the resulting LST map was an intermediate step to assure the data reliability for the further proceeding. After the identification of UHI hot spots in Vienna, the area, where the greening scenarios would be applied in a later step, was to be determined in relation with the LST outcomes. Thereafter, a land use/land cover map of the designated area served as base for the scenario analysis. Different greening scenarios were generated by increasing the green share. Both the land cover map and the modified land cover maps for each scenario were needed as main model input for the InVEST urban cooling model. Further data had to be gathered and preprocessed to meet the model data input requirements. By running the model, heat mitigation index rasters were produced, which were evaluated in order to answer the overall research question. By also changing model parameters, the sensitivity of the urban cooling model was evaluated.

4.2 THERMAL DATA ACQUISITION

Finding appropriate remote sensing data with relatively high spatial resolution and availability at nighttime was very challenging, especially when looking for freely available imagery. However, a lot of research and the guidance of an expert led to the choice of NASA's ECOsystem Spaceborne Thermal Radiometer Experiment on Space Station (ECOSTRESS). ECOSTRESS was launched in June 2018 and provides thermal imagery in cities at 70 x 70m resolution. The acquisition time varies, which enables to have data for different times of the day, every 3-5 days on average over most of the globe (Shi et al., 2021). The instrument contains a multispectral whiskbroom scanner with five spectral bands in the TIR between 8 and 12.5 µm and an additional band at 1.6 µm for geolocation and cloud detection (Hulley at al., 2019 & Silvestri et al., 2020). ECOSTRESS offers a number of higher level products, such as LST data, cloud mask or emissivity. Some key imaging characteristics make ECOSTRESS uniquely suitable for observing the urban environment. Besides, the high resolution of 70mx70m which is approximately the size of a football field, the inclined, precessing ISS orbit allows for samples of temperatures and heat stress at different times of a day. Moreover, the five thermal bands on ECOSTRESS enable the implementation of multispectral temperature/emissivity separation approaches like the TES algorithm (Hulley et al., 2019). ECOSTRESS thermal data can be freely downloaded from the data portal of the United States Geological Survey (USGS), called Earth Explorer in HDF5 format, or ordered at the data portal Application of Extracting and Exploring analysis Ready Samples (AppEEARS) as geotiff.

4.3 FILTERING BY TROPICAL NIGHTS

In order to focus on heat islands during tropical nights in this thesis, information on the exact dates of tropical nights in Vienna was needed prior to download the suitable remote sensing data. Knowing that remote sensing data will not be available for any designated night, as well as tropical nights occur only on several nights during summer months, chances to find a match of both would be higher when including at least three summer periods. The information of tropical night dates was delivered by the "Zentralanstalt für Meteorologie und Geodynamik" (ZAMG) which provides meteorological and geophysical services for Austria. The provided information included minimum temperature measurements for seven different weather locations in Vienna, starting at January 1st 2019 until December 31st 2021. The temperature measurements were taken in 2m height from ground and show the temperature minimum from the day before 7pm until 7pm CET. The map below shows the exact locations of the weather stations, which are distributed over the city of Vienna.

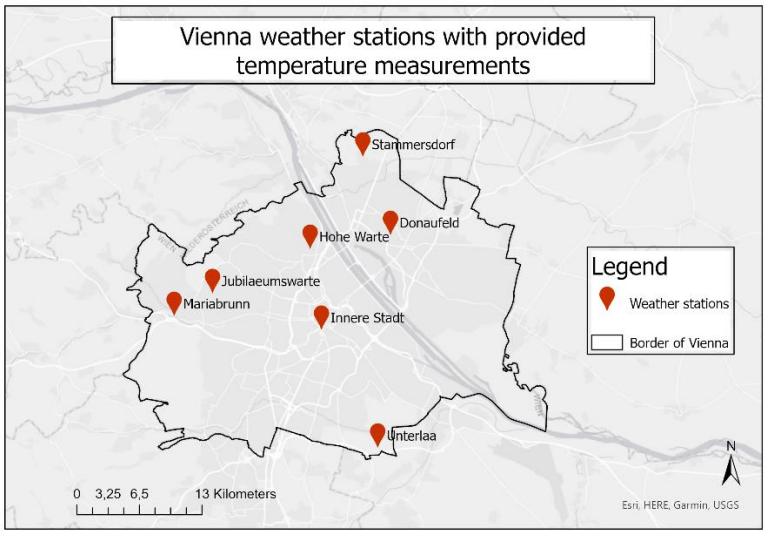

Figure 5: Location of weather station with provided minimum temperature measurements

To obtain the dates for tropical nights, the first step was to filter the dates when the minimum temperature value reached 20°C or more. As temperature measurements vary slightly among the seven weather stations, dates were rated sufficient for a tropical night when one of the locations showed a value of 20°C or more. The filtering led to 87 dates when a tropical night occurred at least at one of the weather stations. The next step was to check the availability of ECOSTRESS thermal data for these 87 dates. In case of a match, an acquisition time during nighttime was another requirement. As the coldest time of a tropical night is usually before sunrise, the boundaries were set from midnight to 7am. This step was carried out manually in Earth Explorer, where ECOSTRESS data can be viewed before download. Since images are taken at universal time (UTC), two hours had to be added for Central European Summer Time (CEST). Further criteria to be kept in

mind were the avoidance of cloud cover and the covering of the whole study area on one thermal image. The exclusion of cloud cover can be set directly in the filtering options of Earth Explorer. Accordingly, the filtering resulted in 15 dates with available data and simultaneously the occurrence of a tropical night based on at least one weather station as shown in table 1, where temperature minimums of 20°C or more are marked in red.

Date	HOHE WARTE tmin [°C]	INNERE STADT tmin [°C]	STAMMERS-DORF tmin [°C]	JUBILÄUMS-WARTE tmin [°C]	MARIABRUNN tmin [°C]	UNTERLAA tmin [°C]	DONAUFELD tmin [°C]
27.06.2019	23,2	25,9	21,6	24,2	19,0	22,5	23,1
01.07.2019	19,9	22,6	18,3	18,5	17,6	20,3	19,7
26.08.2019	18,3	20,1	17,8	18,4	16,0	18,0	18,6
28.08.2019	19,6	21,6	18,8	18,9	18,0	19,3	20,1
29.08.2019	19,1	21,3	17,6	19,6	15,8	18,4	19,2
28.06.2020	19,1	21,3	18,0	18,8	16,9	18,7	19,4
05.07.2020	18,8	20,2	18,0	15,7	12,2	17,2	18,3
06.07.2020	18,8	21,1	18,0	18,1	15,4	18,9	19,5
10.07.2020	16,6	19,7	14,9	20,4	14,4	17,1	17,1
22.08.2020	18,4	21,0	17,2	18,9	16,3	18,8	19,1
22.06.2021	20,0	22,4	18,2	18,9	18,3	19,7	20,3
23.06.2021	21,5	22,1	21,0	18,8	19,8	20,7	21,7
28.06.2021	17,8	21,1	16,5	19,0	14,3	18,9	18,4
07.07.2021	21,6	22,2	20,6	19,0	20,4	21,3	22,3
08.07.2021	19,1	20,5	18,4	16,8	17,6	19,3	19,8

Table 1: Temperature minimum ≥20°C at seven weather stations in Vienna; source: ZAMG

Eventually, the image from July 7th 2021 was chosen, as it shows a clear sky in the preview of Earth Explorer and 6 out of 7 weather stations measured a tropical night then. The data was downloaded from the data archive Earth Explorer in Hierarchical Data Format (HDF). Even though, this data format comes with an additional preprocessing step, the download was quicker than at the AppEEARS data portal. And moreover, it came with an additional raster layer, showing low quality pixels for exclusion.

4.4 Image processing

The first part of the image processing was conducted in Matlab, in order to open the downloaded HDF5 file, which is not supported in ArcGIS. The whole Matlab script is added in Appendix A. After reading the file, low quality pixels were extracted from the data. This step is applied to ensure that error pixels and pixels cloud-contaminated pixels were excluded. As mentioned before, the HDF5 file came with additional data, namely quality flag (QF) and quality control (QC) data which were used to show and remove unreasonably low LST values (Chung et al., 2020). The next step, that was applied in Matlab, was the cropping to the study area, as the

downloaded raster layer covers a much bigger area. And finally a raster in geotiff format was produced and written to a file.

The last image processing step encompassed the transformation from raw data to temperature values in degree Celsius, since ECOSTRESS offers already calculated LST data. This step was done with the formula below in ArcGIS, where C is the Celsius temperature and DN (digital number) represents the value of the raw LST data. The latter is multiplied with the scale factor minus 273,15 to get Celsius from Kelvin (Chung et al., 2020).

$$C = DN * 0.02 - 273.15$$

4.4.1 ECOSTRESS LST product

LST and spectral emissivity are the two primary Level-2 products of ECOSTRESS that are generated by ECOSTRESS TIR data. The emitted surface radiance from the Earth's surface is dependent on both LST and emissivity and thus presents quite a difficulty. Even with well-known atmospheric properties (water vapor and air temperature) LST and emissivity retrieval from multispectral measurements is still a non-deterministic process. This is because the total number of measurements (N bands) is always less than the number of unknown variables (emissivity in N bands + LST). Hence, temperature and emissivity separation approaches will never be perfectly done, and errors may occur. To overcome this gap, ECOSTRESS Level-2 products use a non-deterministic approach, where spectral variations in the retrieved emissivity can be related to surface composition and cover, in addition to the retrieval of surface temperature. The so-called Temperature Emissivity Separation (TES) algorithm is a hybrid algorithm that capitalized on the strengths of previous algorithms to retrieve temperature and a full emissivity spectrum (Hook, 2011).

4.5 IMAGE SHARPENING

Satellite-derived LST retrieved from thermal infrared (TIR) tend to have a coarser spatial resolution than surface reflectance data collected from shortwave bands on the same instrument (Xue et al., 2020). Moreover, thermal imagery either comes with high temporal resolution but low spatial resolution or at a higher spatial resolution but a low revisit time. To bridge this gap, attempts have been made to downscale low spatial resolution thermal images for further use and applications. Besides temperature unmixing methods, thermal sharpening is a widely used approach. Sharpening methods for thermal imagery are based on a correlation between thermal images and auxiliary data like NDVI, emissivity, albedo, digital elevation model or NDMI (Huryna et al., 2019). Satellite TIR resolutions may resolve the scales of urban-rural LST differences, but it is not sufficient to resolve most urban features, like roads and buildings, to study microclimates and human comfort in urban areas

Visible and near Infrared (VNIR) data come generally with a higher resolution than TIR as a consequence of their shorter wavelength. First attempts for image

sharpening leveraged higher resolution VNIR data by relating LST to the normalized difference vegetative index (NDVI). Further methods make use of a simplified fractional vegetation cover, emissivity or topographic variations, but they all come with disadvantages for urban areas. In urban areas, solar reflectance (albedo) has found to be another determinant of LST. Especially within unshaded land classes, albedo correlates well with LST (Dominguez et al., 2011). Dominguez et al. (2011) suggest an approach called high-resolution urban thermal sharpening method (HUTS), which takes into account NDVI and albedo from the VNIR channels.

In this thesis the HUTS method was applied to the coarse LST data. The idea was to increase the spatial resolution from 70m to 30m by the use of a Landsat surface reflectance image. The whole process was based on a tutorial published by Hello World Labs, which is a network of world-class experts in software development, environmental data, sensor hardware and behavior-change design (helloworlde, 2022). The image sharpening was conducted using Matlab (see Appendix B). Before applying several calculation steps in Matlab, a matching image to the ECOSTRESS LST had to be found. Since Landsat has a revisit time of 16 days and the image needed to be cloud-free, it was very unlikely to find an image of the same day and year. Regarding this, a Landsat 8 image from July 20th 2021 turned out to be the best choice. For the calculations of NDVI and albedo, only band 2 (Blue), band 4 (Red), band 5 (NIR), band 6 (SWIR 1) and band 7 (SWIR 2) were needed.

NDVI is the most common used vegetation index (Rasul, 2018). It calculates the balance between the energy obtained and emitted by objects on earth (Hashim et al, 2019). Being ratio-based, it uses only two bands, to recognize healthy flora and green biomass differences, as seen in the equation below. NDVI values cover a range between -1.0 and +1.0, whereas high NDVI values of about 0.6 to 0.9 are related to dense vegetation. Inanimate objects like bare soil or build up areas come with a low value on the other side of the scale (Rasul, 2018).

$$NDVI = (band5 - band4)/(band5 + band4)$$

$$Albedo = ((0.356*band2) + (0.130*band4) + (0.373*band5) + (0.085*band6) + (0.072*band7) -0.0018)/1.016;$$

The factors which are multiplied with each band are specific multiplicative rescaling factors from the metadata. The divisor is the sum of all band-specific multiplicative rescaling factors from the metadata.

The next step for the image sharpening in Matlab was resizing the produced NDVI raster and albedo raster to the extent of the ECOSTRESS image. Thereafter, the fitting coefficients to model low-resolution LST with albedo and NDVI were specified and applied for training (Hulley, n.d.). Only low-resolution surface temperature is available for training the relationship between surface temperature vs. NDVI and

albedo, when applying sharpening techniques to satellite data (Dominguez et al., 2011).

For this thesis the suggested coefficients from the tutorial were adopted, as they were suggested to be used for ECOSTRESS LST. In the next step, the difference between the observed ECOSTRESS LST and the calculated low-resolution fit was calculated, which was used as input in the further step. The subsequent part was targeted to smooth the image by building matrices that computed running sums. While one matrix was designated to smooth along the rows, another was created to smooth along the columns. The smoothing was applied over 2x2 pixels. Not-a-number (NaN) pixels were set to zero to not cause any distortions in the running sums. For each 2x2 element the number of NaN pixels had to be counted and excluded from the division values for calculating means. Finally, the actual image sharpening was conducted by first specifying the high-resolution sharpening LST fit and then resizing the smoothened image with the nearest neighbor algorithm. The calculated, sharpened LST image was directly written to a file (Hulley, n.d.).

4.6 In Situ validation

When using satellite image-based surface temperature data for heat island studies in urban areas with complex spatial characteristics, essential factors that influence surface temperatures must be considered comprehensively. These factors comprise the coverage texture type, the color of the surface layer, sky view factors, street geometry, traffic loads and other anthropogenic activities. To allow for diagnosing UHIs more accurately and preparing appropriate relief plans, it is indispensable to validate the accuracy of satellite image surface temperature data by comparing it to in situ surface temperature data (Song & Park, 2014). These so-called temperature-based (T-based) methods are rather simple compared to radiance based (R-based) methods and therefore widely used to validate remotely sensed LST products at homogeneous stations. As urban areas are heterogeneous in topography, physical structures or land use, to name a few, averaging of the LST temperature over a larger buffer zone may drown out the physical noise that can influence the air temperature at a specific point (White-Newsome et al., 2013). White-Newsome et al. (2013) found that correlations between LST and in situ measurements were stronger at larger buffer radii, such as 500m or 800m.

In situ surface temperature data was delivered again from ZAMG, which provided a link to their data hub, where hourly temperature data for each day of the past few years are accessible. However, the temperature data encompassed only measurements for seven different weather stations, like shown in figure 5. Since this was insufficient to prove the accuracy of the used LST ECOSTRESS image, the decision was made to use a bigger extent (~160km x 120km) of the downloaded LST ECOSTRESS tile, which resulted in 43 ground stations to be available for comparison, as indicated in figure 6. The downloaded dataset came with twofold measurements, air temperature measured at a height of 5cm and air temperature measured 2m above ground. Both values were compared to the LST raster layer. As

suggested by White-Newsome et al. (2013), buffer zones of 500m and 800m were calculated around each weather station location. Mean raster values were then calculated with zonal statistics in ArcGIS, which were to be compared with the in situ measurements.

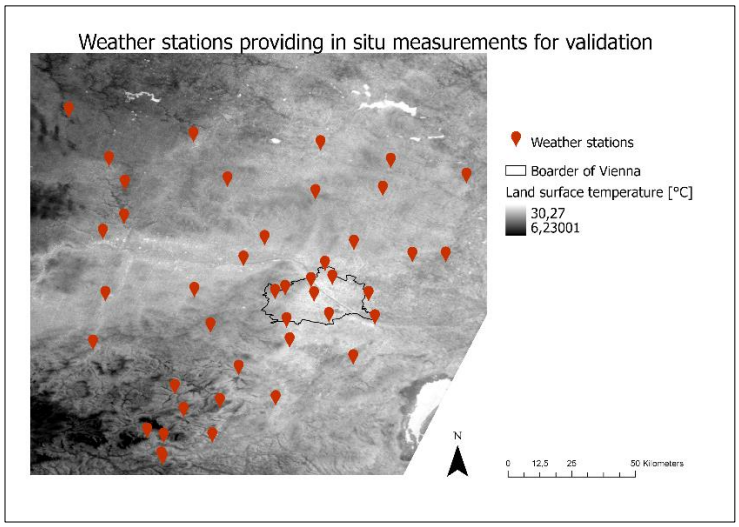

Figure 6: Weather station locations that provided in situ measurements for validation

4.7 SCOPE DEFINITION OF HOT SPOTS

Since the target of this master thesis is the heat hot spot area of the previous land surface temperature calculation, this hot spot area had to be defined first to proceed with the next steps. Mean temperature values were calculated for all districts of Vienna, as well as mean temperature values for Vienna's census districts to have more detailed information on certain neighborhoods. Based on the outcomes, which are indicated in chapter 5, the district "Josefstadt" was chosen to be the focus area for the scenario modelling.

4.8 INVEST URBAN COOLING MODEL

One of the most advocated strategies to mitigate urban heat, is the increase of urban green space, especially the urban tree canopy. However, the impacts of the urban tree canopy on air temperature indicate a complex spatial behavior that remains poorly understood. The cooling effect of urban green areas has been widely reported, while the relationship between their size and their cooling capacity is nonlinear. Thus, little is known about the overall spatial configuration of green spaces in connection with heat mitigation, which makes urban green infrastructure planning quite a challenge (Bosch et al., 2021).

Bosch et al., (2021) introduces a new approach to address the above-mentioned shortcomings. Integrated Valuation of Ecosystem Services and Tradeoffs (InVEST) is a software suite that models the links between nature and the well-being of humans. Overall, it has been widely used to indicate the potential of natural

infrastructure investments with different scopes. Some new tools of InVEST focus on urban areas, addressing urban cooling to reduce the urban heat island effect among others. What makes it an appealing instrument is, that InVEST urban tools are free, open-source, and modular, which enables users to choose which services to include in the analysis. The tools are designed to combine spatial information about natural infrastructure's benefits with resilience research and practice (Hamel et al., 2021).

The tool used in this research is the InVEST urban cooling model, a method that aims to evaluate the heat mitigation potential of altering the abundance and spatial configuration of the urban tree canopy cover. There are two main steps in this method. First, synthetic scenarios are generated by rising the tree canopy cover where the urban fabric permits it. Thereafter, the spatial distribution of air temperature of each scenario is estimated with the inVEST urban cooling model. The original model simulates urban heat mitigation based on three biophysical processes, which are shade, evapotranspiration and albedo (Bosch et al., 2021). However, there is another method designated for nighttime heat mitigation, which is based on building intensity instead of shade and albedo. Since this thesis focuses on tropical night UHI, the nighttime approach was chosen.

The heat mitigation index indicates the ability for an area to regulate temperature. Areas with a high heat mitigation index will be more resilient to the higher temperatures derived from UHI. This index is especially beneficial to urban planners to promote heat mitigation initiatives, such as white roofs and green spaces, to low-score heat mitigation areas. The understanding of factors that influence the cooling capacity the most, will improve future efforts to target the UHI effect and build community resilience (ArcGIS StoryMaps, n.d.).

4.8.1 Generation of greening scenarios

One of the requirements for the InVEST urban cooling model was a land use/land cover (LULC) raster layer, which also served as basis for the generation of greening scenarios. A LULC shapefile from 2018 was downloaded from Copernicus' Urban Atlas which provides reliable, inter-comparable, high-resolution land use and land cover data for 788 urban areas with more than 50 000 inhabitants within the European continent. Urban Atlas originated as a joint initiative in the frame of the EU Copernicus program (Copernicus Europe's eyes on Earth, 2022).

Dataset	Year	Source	Description	Data type
AT001L3_WIEN_UA2012	2018	Urban Atlas - Copernicus Programme	Land use layer for Vienna	shapefile
BEZIRKSGRENZEOGDPolygon	2020	Open data Österreich - Stadt Wien	District boundaries of Vienna	shapefile

Table 2: Used datasets for the land cover maps

The derived LULC map from the Urban Atlas is indicated in figure 7 in the top left corner. It served as the basis for the scenario modelling. The idea was to modify the shapefile manually in ArcGIS by simply changing polygons with the attribute "Continuous urban fabric" or "Industrial, commercial, public, military and private units" to "Green urban areas".

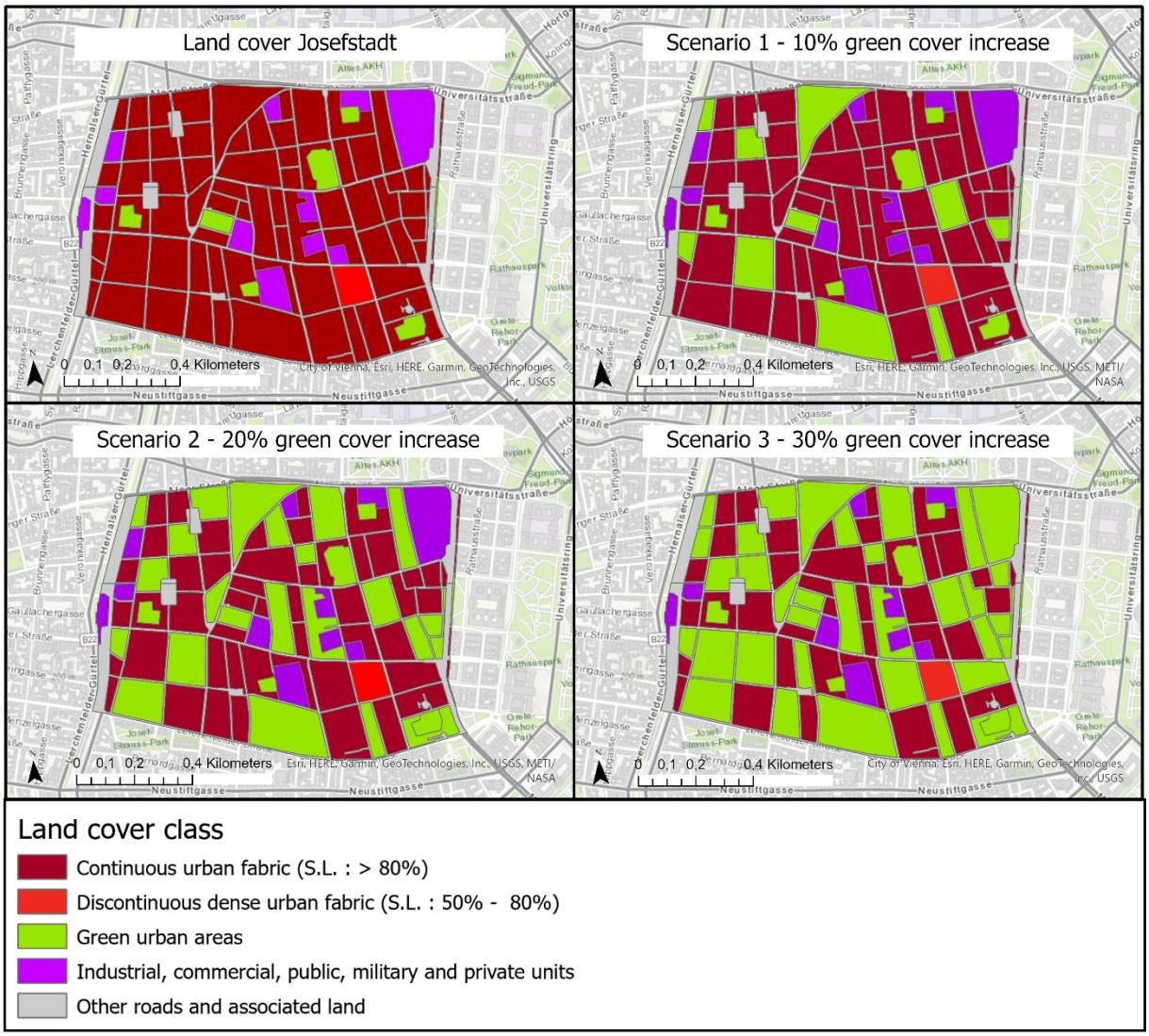

Figure 7: Land cover and land cover scenarios for Josefstadt

"Continuous urban fabric" describes areas with more than 80% building density, while "Discontinuous dense urban fabric" ranges between 50% and 80%. The latter is assigned when urban structures and transport networks associated with vegetated areas and bare surfaces are available and they occupy significant surfaces in a spatial pattern. Other features like buildings, roads and artificially surfaced areas concern 50% to 80% land coverage (Copernicus Europe's eyes on Earth, 2022). Since these areas come with a certain proportion of green share, they were not converted to green areas in the greening scenarios. In contrast,

"Industrial, commercial, public, military and private units" was used for the generation of greening scenarios. Even though the actual percentage of vegetated areas remains unknown for this class, it is described as an area mostly occupied by buildings, other built-up structures and artificial surfaces. Unlike "Continuous urban fabric" this class is assigned for land units that are under industrial or commercial use or serve for public service facilities (Copernicus Europe's eyes on Earth, 2022).

To evaluate the sensitivity of the InVEST urban cooling model, three greening scenarios were generated. 10%, 20% and 30% increase of green cover was chosen to be mapped in scenarios, to make temperature change apparent. Even though it seems very unlikely for Josefstadt to rise its vegetated area by 30%, the idea was to simply show the impact of enhanced vegetation in dense urban areas.

To make sure that green land cover is increased by the designated percentage, the land cover classes of Josefstadt's land cover map were summed up and its percentages calculated. This led to an increase of approximately 15,64ha for 10%, meaning that polygons with the attributes "Continuous urban fabric" or "Industrial, commercial, public, military and private units" needed to be converted to "Urban green areas" until the 15,64ha gain was reached. For the further two scenarios, a 20% and a 30% increase, equaling 31,28ha and 46,92ha was conducted, as indicated in figure 6.

4.8.2 Evapotranspiration

Evapotranspiration (ET) measures the amount of water that vaporizes from land into the air over a certain period of time. It contains the sum of both evaporation and transpiration. The former describes the process whereby liquid water is converted to water vapour and removed from the evaporating surface. Evaporation occurs from a variety of surfaces, like lakes, rivers, pavements, soils and wet vegetation. Transpiration on the other hand comprises the vaporization of liquid water contained in plant tissues and the vapour removal to the atmosphere. Evapotranspiration as the combination of both processes is typically expressed as a depth of water in millimeters per unit time, like mm/month or mm/year (InVEST documentation, 2022). Urban areas, with expansive impervious surfaces, have generally more runoff than their rural counterparts. As the runoff water drains quickly, in the long run, less surface water remains available for evapotranspiration, which affects the urban surface energy balance (Taha, 1997). Qiu et al. (2013) even proposed that vegetation evapotranspiration has great potential to reduce urban and global temperatures, and that vegetation and urban agricultural ET can reduce urban temperatures by 0.5 to 4.0°C (Qiu et al., 2013).

For this research evapotranspiration input data were retrieved from ECOSTRESS satellite data. Similar to land surface temperature, which was used in an earlier step, an evapotranspiration raster can be downloaded freely via Earth Explorer or AppEEARS as a fully calculated data product for numerous days a month. Evapotranspiration imagery comes with the same spectral resolution as LST, which is 70m. In fact, evapotranspiration, which is produced as Level-3 latent heat flux

data product, is generated from land surface temperature and emissivity, combined with ancillary surface and atmospheric data (Fischer et al., 2020).

Dataset	Year	Source	Description	Data type
ECO3ETPTJPL.001_EVAPOTRANSPIRATION _PT_JPL_ETdaily_doy2021188040608_aid000	2021	AppEEARS data portal	Evapotranspiration raster for Vienna region	geotiff
BEZIRKSGRENZEOGDPolygon	2020	Open data Österreich - Stadt Wien	District boundaries of Vienna	shapefile

Table 3: Used datasets for evapotranspiration

4.8.3 Biophysical table

A biophysical table in CSV format was needed as further InVEST model input. The documentation of the InVEST urban cooling model specified requirements for this table. Besides the linkage to the LULC map of the designated area by indicating each LULC code, three attributes needed to be indicated for each LULC class. A crop coefficient had to be assigned to each LULC class, as well as the indication of green area or non-green area. And finally, the building intensity for each LULC class had to be determined.

4.8.4 Crop coefficient

The crop coefficient Kc incorporates crop attributes and averaged effects of evaporation from the soil. For most planning and management purposes and for most hydrologic water balance studies, average crop coefficients are adequate (Allen et al., 1998).

Liu & Shen (2018) and Kuriata-Potasznik & Szymczyk (2016) suggest a crop coefficient of 1.04 and 1.05 respectively for grassland during mid-season of its growth. For trees that typically grow in Viennese parks, like beeches, maple trees or lime trees, such crop coefficients were not found in literature. In addition, comparable trees were lacking too. Accordingly, the used crop coefficient for the LULC class "Green urban area" was adopted from the suggested grassland values found in literature.

For non-vegetated LULC the InVEST documentation suggests approximations of Kc, which are based on Allen et al. (1998). Even though these values may not be fully accurate, the impact on model results should be minimal, unless the LULC represents a significant portion of the watershed (InVEST documentation, 2022). Since the 8th district of Vienna appears relatively homogenous with relatively little LULC classes, only the Kc value for built areas was relevant from the non-vegetated exceptions to be estimated. According to InVEST documentation (2022), kc can be determined with the following formula.

$$Kc = f*0.1 + (1-f)*0.6$$

Variable f is the fraction of impervious cover in the area. For built areas, evapotranspiration from pervious areas is assumed to be nearly 60% of reference evapotranspiration. However, evaporation from impervious surface is assumed at 10% of PET (InVEST documentation, 2022).

4.8.5 Green area

Another part of the biophysical table inputs is the indication of each LULC class whether to be considered a green area or not. Non-green areas got the value 0, while green areas are referred to with a 1. This attribute is relevant as green areas larger than 2 hectares have an additional cooling effect (InVEST documentation, 2022).

4.8.6 Building intensity

To complete the biophysical table as input for the InVEST urban cooling model, the building intensity for each LULC class had to be determined. The building intensity describes the ratio of building floor area to the footprint area (The Natural Capital Project, 2022). In literature, this ratio is known as Floor Area Ratio (FAR), an essential measure of the capital-land ratio in urban areas (Barr & Cohen, 2014). As indicated in Figure 8, it is calculated by multiplying the building area with the number of floors and dividing that by the total area. To receive a representative FAR value for each LULC class, FAR was actually calculated for the 8th district of Vienna. The idea was to determine mean values for each LULC class to be used in the biophysical table.

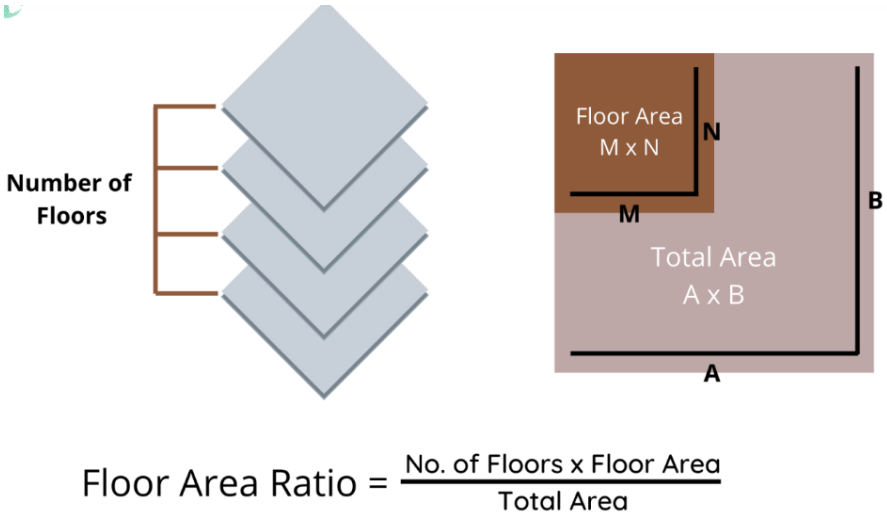

Figure 7: Illustration of Floor Area Ratio (Liveup Homes, 2020; https://liveup.in/blogs/floor-area-ratio-far-explained/)

For the calculations several datasets were retrieved. The geodata viewer of the city of Vienna was used to obtain several shapefiles with the building footprints, which also provided area and height information of each building. The height information of each building area was received through arial imagery. Hence, it doesn't align with the building height according to the Viennese building code (Stadt Wien, 2022).

Dataset	Year	Source	Description	Data type
main.CP_CadastralParcel	2021	Federal Office of Metrology and Surveying	Land register for Austria	shapefile
101081_bkm	2019-2021	Geodatenviewer der Stadtvermessung Wien	building footprint for each map tile with height information	shapefile
102081_bkm	2019-2021	Geodatenviewer der Stadtvermessung Wien		
103081_bkm	2019-2021	Geodatenviewer der Stadtvermessung Wien		
103082_bkm	2019-2021	Geodatenviewer der Stadtvermessung Wien		
103083_bkm	2019-2021	Geodatenviewer der Stadtvermessung Wien		
102083_bkm	2019-2021	Geodatenviewer der Stadtvermessung Wien		
101083_bkm	2019-2021	Geodatenviewer der Stadtvermessung Wien		
101082_bkm	2019-2021	Geodatenviewer der Stadtvermessung Wien		
102082_bkm	2019-2021	Geodatenviewer der Stadtvermessung Wien		

Table 4: Used datasets for building intensity

Since the dataset showed all building surfaces with different heights as separate polygons and causing very small polygons withing buildings, all related building areas were merged in ArcGIS with the dissolve function. The challenge then was to get suitable height information when merging related areas. Looking at the original dataset, the heights of the smallest polygons tended to either show really high or extremely low heights (e.g. portals). Accordingly, the mean height value was chosen for the merged areas.

To calculate FAR, the number of floors was needed, which led to another estimation in this process, as only the total height of the buildings was known. Josefstadt is predominated by buildings from the so called "Gründerzeit" between 1848 and 1918, leading to floor heights between 3,20m and 4m. Since the heights of ceilings between the floors comprise around 40cm (Psenner, 2014), a total floor height of about 4m was estimated. Hence, the total building height of each building was divided by 4 to get the approximate number of floors for each building.

Another dataset was needed for the total plot area, which was found at the data portal of the Federal Office of Metrology and Surveying (BEV). It provided land register information for big parts of Austria and was clipped in a first step to the extent of Josefstadt.

Accordingly, the two datasets with the register information and the building area information needed to be joined to finalize the FAR calculation. This step was conducted with a spatial join in ArcGIS (see figure 12), where one object is joined to one other object, since related buildings were already merged to multipart features. Since streets and very small cadaster polygons led to false output data, those data were excluded from the dataset. After the FAR calculation, a random manually check on the data was made, leading to the exclusion of some extreme values. Further validation of the output was not part of the scope of this thesis.

Figure 8: From left to right (1) building footprints with height information; (2) land register parcels; (3) spatially joined datasets with calculated FAR, where darker colors mark higher values

Calculating mean values for each LULC class from the calculated FAR layer was one of the last steps for completing the biophysical table inputs. This part was simply conducted in ArcGIS by selecting a particular LULC class, clipping the FAR layer to this extent and using the summarized statistics function to determine the mean. This step was applied for all LULC classes except for the class "Other roads and associated lands" which contains mostly streets, pavement and parking lots within the area of Josefstadt, but no buildings. Accordingly, a FAR value of 1 was assumed for this category, as it covers mostly sealed areas.

As the biophysical table for the InVEST urban cooling model input required a normalized value for each LULC class, the dataset was normalized to a range between 1 and 0 with the equation below. X_{min} and X_{max} mark the lowest and highest value within the data distribution.

$$X_{norm} = (X - X_{min})/(X_{max} - X_{min})$$

The complete biophysical table is indicated in figure 12, where lucode 1 to 5 represent the different LULC classes in the order of the maps in figure 7. Lucode 0 represents background or noise values of the LULC raster.

lucode	kc	green_area	building_intensity
0	0	0	0
1	0.15	0	1
2	0.425	0	0.62
3	0.104	1	0
4	0.15	0	0.95
5	0.15	0	0.28

Table 5: Biophysical table as InVEST model input

4.8.7 Further model inputs

Finally, a few further model inputs for the InVEST urban cooling model were needed, which are shown in figure 10. "Baseline air temperature" refers to a reference air temperature value in degree Celsius from an area where the urban heat island effect is not observed. As LST was mapped for a scene including areas

around Vienna, the lowest value, namely 15,6°C, was chosen as model input, assuming that this value represents surface temperature for unsealed area without the impact of the UHI effect.

For the "Magnitude of the UHI effect", another model input, the absolute difference from the baseline air temperature to the highest observed LST value was used, which lead to an input of 7°C.

Moreover, "Air Temperature Maximum Blending Distance" had to be determined. This parameter indicates the radius over which to average air temperatures to account for air mixing (InVEST documentation, 2022). The InVEST documentation (2022) recommends a value of 500m to 600m, as some testing in pilot cities in the USA and Europe suggested.

Finally, the "Green Area Maximum Cooling Distance" was needed as further InVEST urban cooling model input. It describes the distance over which green areas larger than 2 hectares have a cooling effect (InVEST documentation). Again, the recommended value of 450m was chosen.

Another model requirement was the use of a projected coordinate system and not a geographic one, like WGS84. For this analysis MGI Austria Lambert was chosen, which is a conformal conic projection commonly used in Austria.

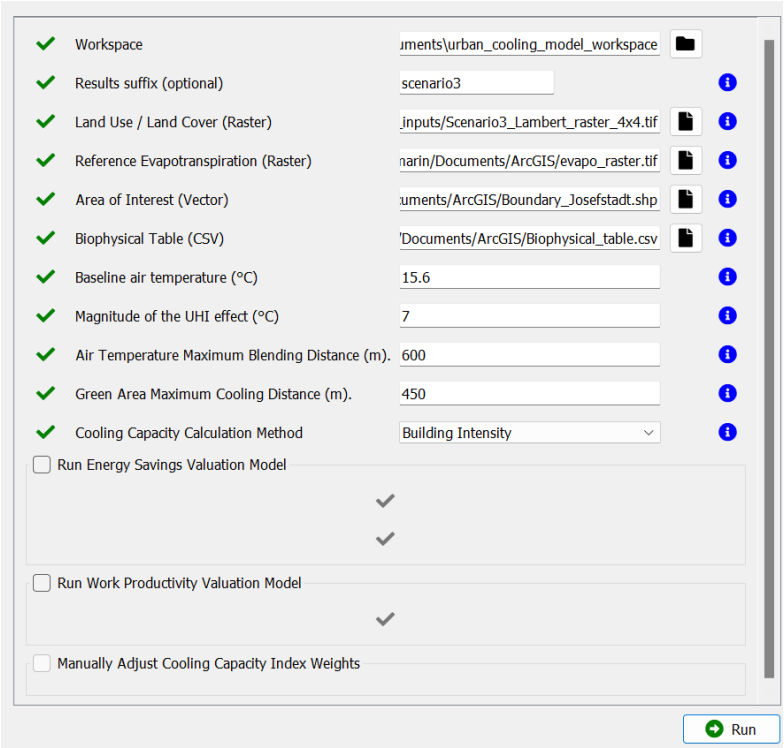

Figure 9: InVEST urban cooling model with examplary data inputs for scenario 3

4.9 Alteration of InVEST model inputs

The sensitiveness of the urban cooling model to different model inputs was evaluated by the alteration of several input parameters. While the different scenarios with the modified LULC inputs could already give information about the sensitivity of the model to green cover change, it was still intended to look at further model inputs and their impact for the outcomes.

Regarding the inVEST urban cooling model inputs, 4 parameters were chosen to be altered, which are listed in table 6. The table illustrates the model requirements with their initial model inputs and the modified values. The modification of some values of the biophysical table would not have been constructive, as these values are bound to each LULC class and changing them would only result in false model predictions.

Model input	Initial input value	Modified values
Baseline air temperature	15.6°C	18°C
UHI magnitude	7°C	9°C
Air Temperature maximum blending distance	600m	200m, 1000m
Green area maximum cooling distance	450m	300m, 600m

Table 6: Table with altered parameters

5 RESULTS

This chapter shows all the outcomes of the performed analysis in order to answer the main objective and the research questions. The results will be presented in chronological order accoring to the order of the research questions and the order of the conducted research.

5.1 NIGHTTIME URBAN HEAT ISLANDS

The first result targets the outcomes of research question one regarding the detection of urban heat islands during tropical nights in Vienna. A map with land surface temperature information was produced for July 7th 2021, as shown in figure 11. The temperature values were classified into 5 classes with 1°C difference to the next adjoining class based on the distribution of the histogram. The classification was done to make it more apparent where to draw the line between tropical night's temperature of 20°C or more and temperatures below 20°C.

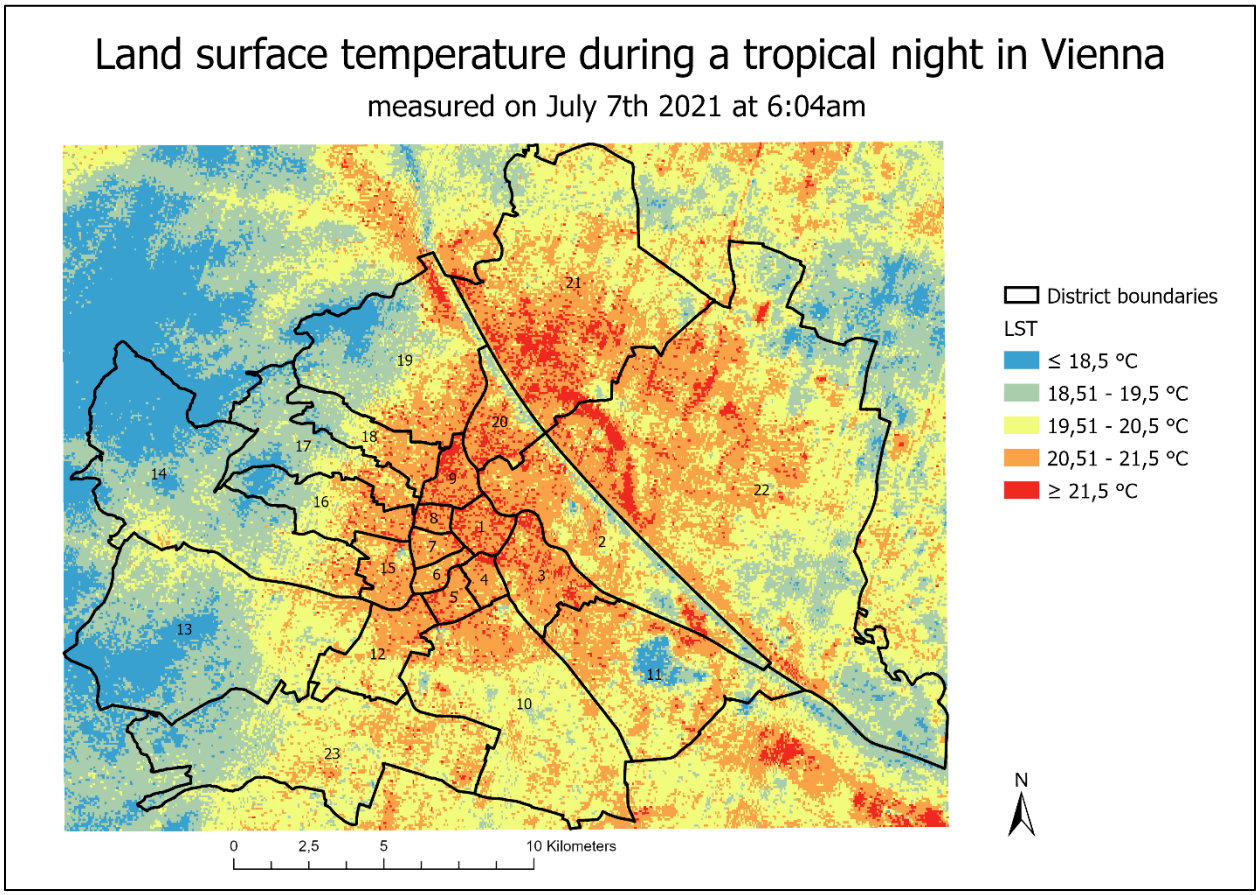

Figure 10: LST map of Vienna

On the first sight, the inner districts of Vienna show higher temperature values than the suburban with temperature values up to 21,5°C and higher. Especially the districts 1, 8 and 9 only seem to have temperature values above 20,5 degrees and

don't show any zones with lower temperatures. However, it has to be kept in mind that the spatial resolution of this map is 70m, and there may be overseen small cooling islands too. Another urban heat island hot spot appears in "Floridsdorf", the 21st district of Vienna, situated across the Danube River. However, only the southern part of Floridsdorf shows very high surface temperatures above 21,5 degrees Celsius, whereas its northern part features lower temperature values. In the bordering 22nd district a curved form is displayed rather clearly with high surface temperature. This is a branch of the Danube River, called the "Alte Donau". Since it is not connected to the Danube River anymore and considered still waters, it can reach very warm water temperatures of 30°C and even more during summertime. Accordingly, this water body appears as one of the surface temperature hot spots in this analysis, unlike the actual Danube River, which is separating the 21st and 22nd districts from the rest of Vienna and causes rather low temperatures. Another distinctive appearance encompasses the western part of Vienna, with an abrupt transition to relatively cold nighttime temperatures. In this area, temperatures reach values equal or less than 19,5°C overall, whereas some areas show values below 18,5°C. The Vienna Woods streche over the Western parts of Vienna, covering this extensive cooling island within Vienna. Another peculiar cool spot within the city of Vienna, emerges in the 11th district. This urban cooling island during a tropical night is mostly covered by greenhouses and cultivated surfaces, which may have a positive impact on the surface temperature.

The histogram in figure 12 shows the distribution of the temperature values. The mean is marked with 19,72°C. Even though there are extreme values with a temperature minimum of 15,63°C and a temperature maximum of 24,37°C, most temperature values occur around the mean.

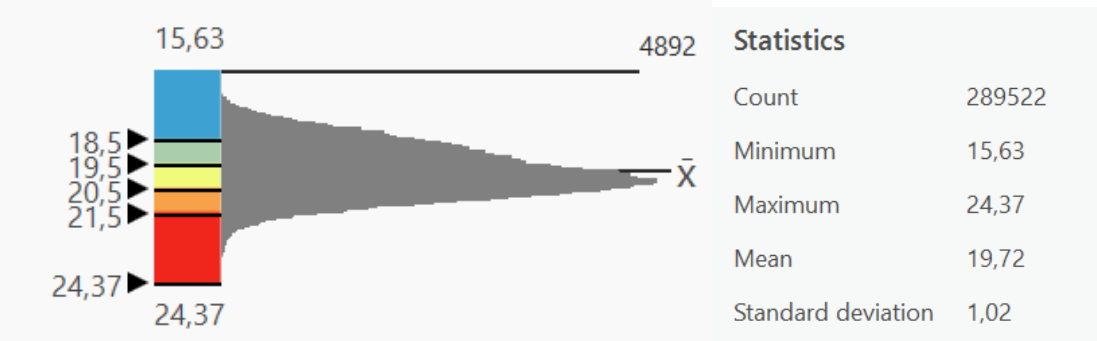

Figure 11: Distribution of the LST values, statistics

5.1.1 Image sharpening

Image sharpening was performed for the LST image in figure 11 in order to get more detailed information, especially for the hot spot areas. However, the analysis did not perform well and produced a pixelated image with apparently a lot of outliers, indicating either very high or very low values. The image is attached in Appendix D. Some elements were pretty clear on the output raster like the Danube River or cultivated areas in the outer districts. The cell size of the calculated LST

raster was definitely minimized, but a detailed look reveals that the cells are rectangles and not 30x30m cells.

The HUTS methodology was suggested for ECOSTRESS LST to be sharpened with Landsat spectral reflectance. Thus, an error in the script seems rather unlikely. Probably, there has been an error in the input data or the calculations of either albedo or NDVI.

Dominguez et al. (2011) states that shaded areas with small surface temperature appear to have a small reflectance as well, which can cause scatter in the surface temperature fit, as the expected relationship between reflectance and surface temperature is not preserved at shaded surfaces. So, it is possible that there may be an error due to shaded surfaces in the albedo raster.

Since image sharpening was not specified in one of the research questions for this thesis, but rather performed to enhance readability of the LST map, no further improvements were made to ensure a good result. Time and the scope of the thesis did not allow for further research here. Therefore, the localization of the most significant urban heat islands in Vienna during a tropical night had to be based on the LST map with 70m spatial resolution.

5.1.2 In situ measurements validation

The validation was performed for the LST ECOSTRESS product, to ensure that the downloaded thermal image is reliable and accurate. As explained in the methodology section of this thesis, buffer zones of 500m and 800m around the weather stations were made, to compare LST mean values with the ground measurements. The whole table, showing the raw outcomes of the validation analysis, is attached in Appendix E, while the results for Vienna are exemplified in figure 17. The overall outcome shows a mean absolute temperature difference of 4,1°C between the station measurements and the LST mean from the 500m buffer. Even though, Vienna had only 7 measure points, this values just deviates by 1°C.

Station number	Station measurements T1 [°C]	LST mean Buffer 500m LST1 [°C]	Absolute difference T1 - LST1 [°C]
5802	20,8	18,4	2,4
5805	23,4	19,8	3,6
5904	24,0	20,8	3,2
5917	24,0	20,3	3,7
4115	23,4	19,8	3,6
5925	23,7	21,3	2,4
5935	24,6	21,0	3,6
Mean	**23,4**	**20,2**	**3,2**

Table 7: Ground measurements in relation to LST means for buffered areas in Vienna

Indicated in figure 13 are the absolute temperature differences between the ground measurements of the 43 weather stations and the means of ECOSTRESS land surface temperature product buffered for 500m around the weather stations. Each number on the x-axis refers to one weather station where the ground measurements derived. The temperature difference between the two dimensions appears comparatively homogeneous overall. Only very few stations seem to have measured much higher or much lower temperatures than observed at the LST raster.

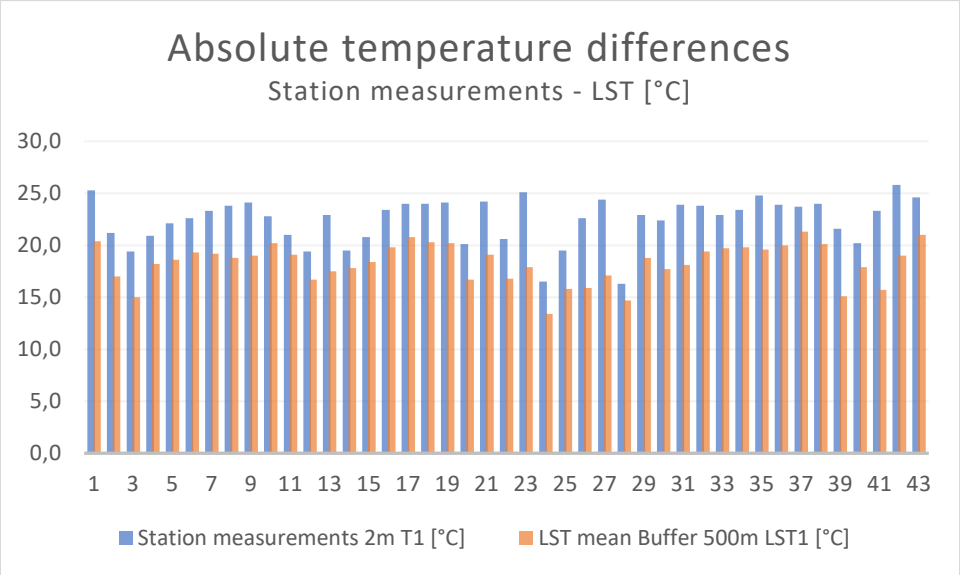

Figure 12: Diagram showing absolute temperature differences between ground measurements and land surface temperature

According to the outcomes of the validation analysis with ground measurements, the ECOSTRESS land surface temperature tends to be collectively lower than the night temperatures measured at 43 weather stations in 2m height.

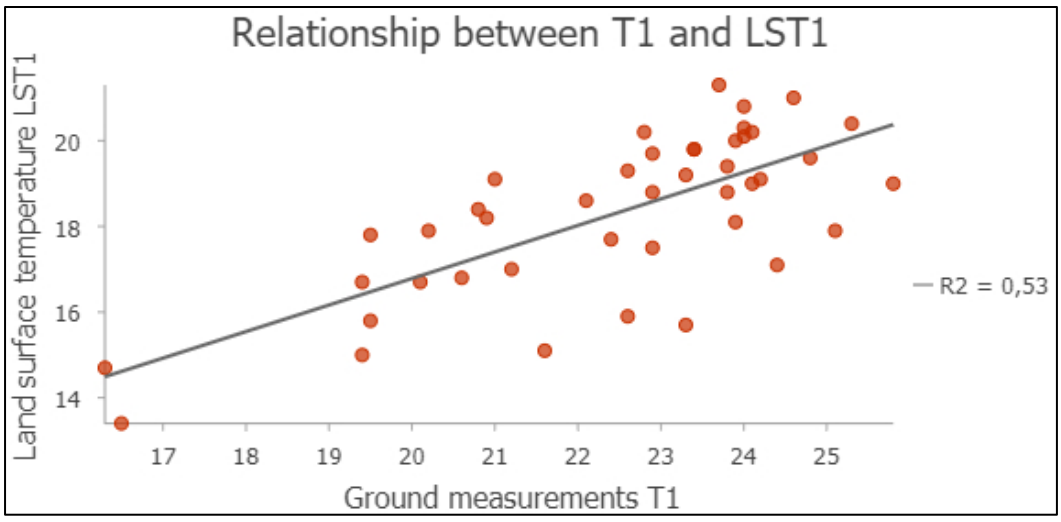

Figure 13: Scatter plot of ground measurements and land surface temperature

With reference to the scatter plot in figure 14, there seems to be a slightly positive linear correlation between land surface temperature and the station measurements. R-squared (R^2) shows a value of 0,53, which indicates a moderate positive correlation.

5.1.3 UHI hot spot identification

Defining the scope of the urban heat island hot spots during a tropical night in Vienna was necessary for further proceeding in this thesis. Since the image sharpening did not turn out as expected, this analysis was entirely based on land surface temperature data with 70m spatial resolution. The LST map of figure 11, gave a first impression of heat and cooling islands of Vienna during a tropical night.

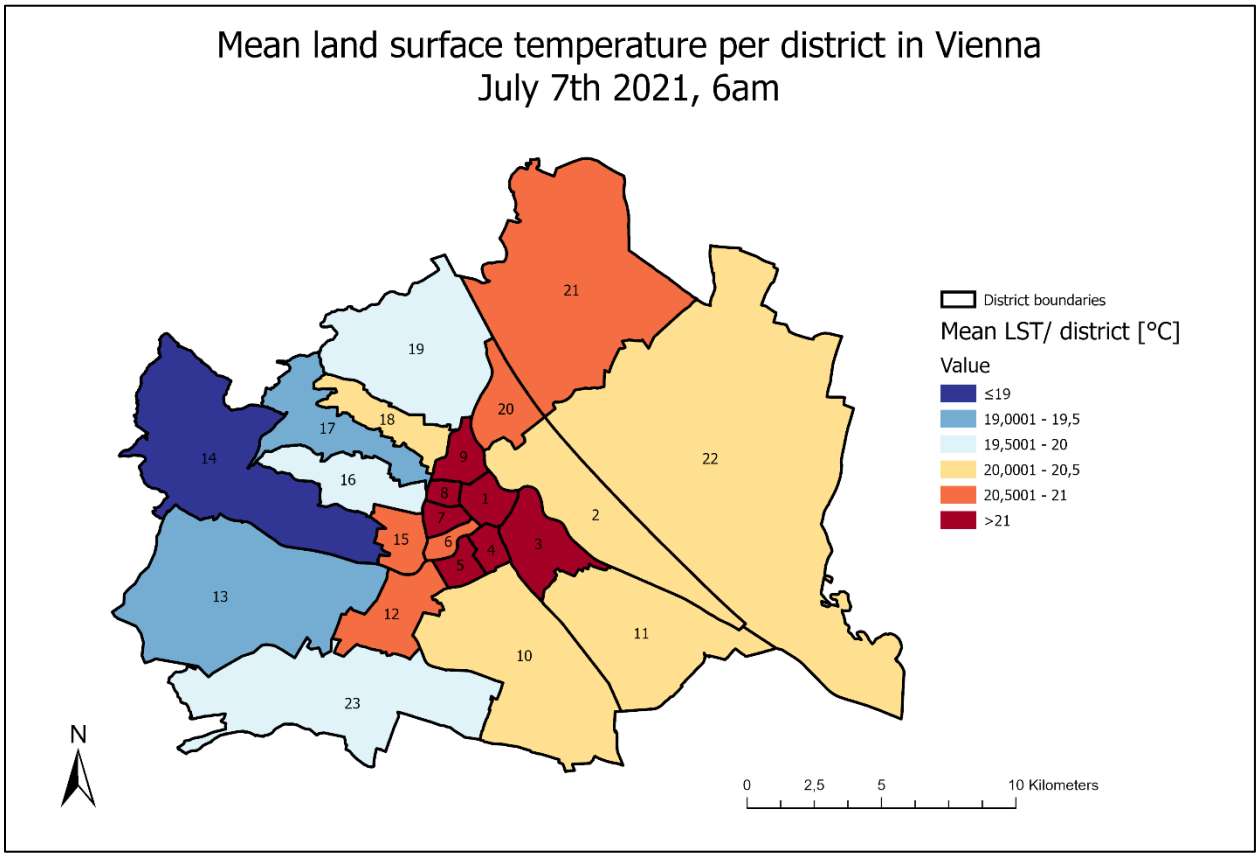

Figure 14: Mean land surface temperature for the districts of Vienna

By calculating mean values for all districts of Vienna, the light was shed to rather large entities of Vienna. However, the map in figure 15 makes the differences between the districts very apparent and significant. Again, the mean values were classified to enhance the comparability of the map. Just as in the LST map from figure 11, the inner districts stand out with the highest mean LST values with average means over 21°C. But besides districts 1,8 and 9, further districts join the hot spot area of the highest land surface temperature. In contrast to that, the western districts, where the Vienna Woods are situated, show once more the lowest mean temperatures. The 21st district in the north, which contained one of the urban

heat island hot spot areas, has an overall mean temperature of 20,5°C to 21°C since the district appeared to have contradictory values from north to south.

A more detailed mean land surface temperature map is shown in figure 16 below, where the census districts were used as entities for calculation. The location of the UHI hot spot areas appear similar to the LST map. Although, the inner districts 1, 8 and 9 show very high mean temperature values of more than 21°C, the 21st district indicates the highest mean values for at least 3 census districts with a mean surface temperature above 21,5°C. A few local heat hot spots can be found in the 16th district or the 5th district, whereas other districts like the 15th or the 10th show an urban cooling island within the city. Temperatures in the 2nd district appear to be very unevenly distributed from north to south, which was not as apparent on the LST map. The lower temperatures in the south-eastern corner of district 2 may be explained by a large closed green space called "Prater".

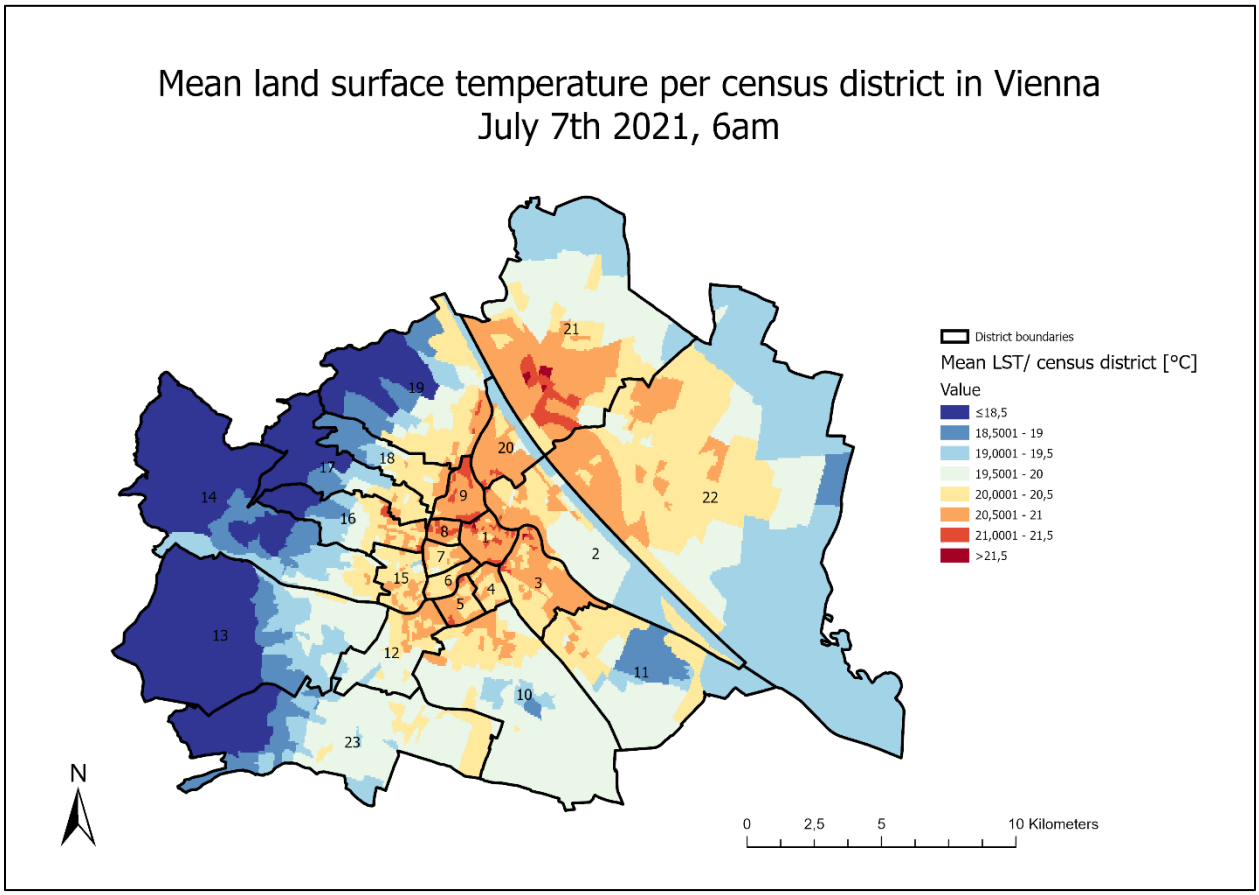

Figure 16: Mean land surface temperature for the census districts of Vienna

Comparing different entities for Vienna concerning the UHI hot spots, a choice had to be made between one of the inner districts or part of the 21st district. Since census districts seemed to be too small to base the upcoming scenario analysis on, the idea was to select one district as focus area. The 21st district seemed too inhomogeneous to choose for further analysis, whereas districts 1, 8 and 9 had

almost identical mean values. Eventually, the 8th district, "Josefstadt" was chosen as focus area, as this district has the lowest green cover rate in the entire city. Only 3% of its land cover are green urban areas (see figure 17). The district is predominated by "continuous urban fabric" with sealed coverage of more than 80%, followed by "other roads and associated land", which is mainly based on streets, pavements and parking lots. Overall, Josefstadt seems to have great potential for improvement regarding urban greening.

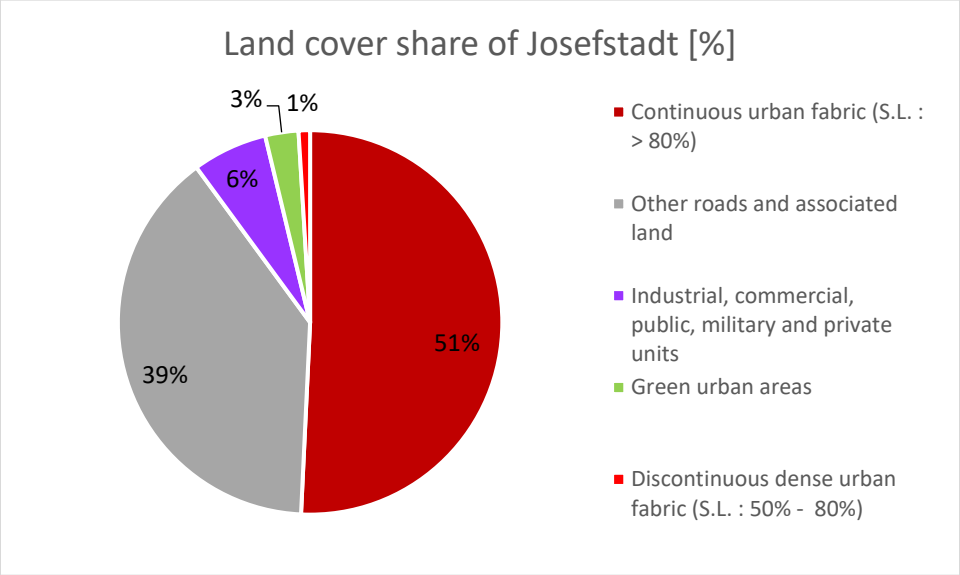

Figure 17: Graph with land cover proportions of Josefstadt

5.2 Scenario analysis

The scenario analysis was targeted to evaluate different greening scenarios for the focus area Josefstadt and answer the overall main objective. An urban cooling index was calculated by use of the InVEST urban cooling model. This index indicates the cooling capacity of an area, which describes the ability of regulating temperature. Figure 18 shows the model outcomes for the actual spatial configuration of Josefstadt, labeled as "status quo" in the left top corner, as well as the outcomes for each scenario. For better comparison the pixel values were classified into 10 classes for index values between 1 and 0. Low pixel values indicate low mitigation potential, whereas high pixel values indicate an excellent cooling capacity of the covered area.

Josefstadt status quo appears to have an extremely low cooling capacity, with large parts showing a heat mitigation potential value of less than 0,1. Streets seem to have surprisingly high values that are only excelled by 6 areas with outstanding high cooling capacity and that refer to parks, when comparing to the land cover map of figure 8. There seems no difference between industrial areas and dense urban fabric regarding cooling capacity within Josefstadt. The area of discontinuous urban fabric also catches the eye as only zone with a moderate urban cooling index value. The strong connection between urban green space and cooling capacity is

already visible in the first map. When increasing the green cover by 10%, it can be observed that the overall cooling capacity within dense urban fabric and industrial areas was increased. The lowest cooling index values are between 0,1 and 0,2.

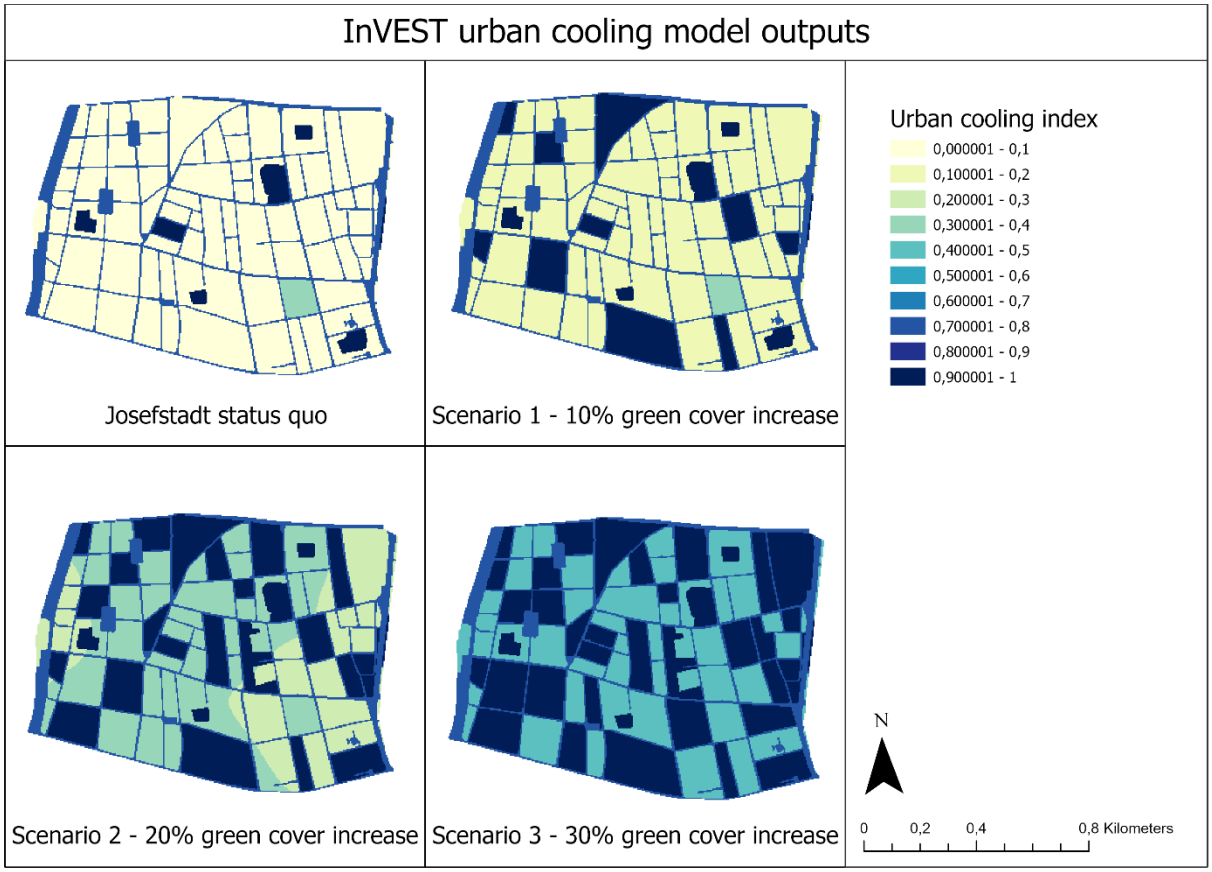

Figure 18: Urban heat mitigation index for Josefstadt, calculated for different scenarios

20% green coverage enhancement, as indicated in scenario 2, leads to more significant changes already. While the urban green areas itself remain with the highest urban cooling capacity, the increased green cover has moderate cooling effects on the whole district, with minimum values of 0,3. The streets are not affected by the bordering green areas. The last scenario, with a 30% green cover increase, has entirely converted the 8th district of Vienna to a region with a rather high heat mitigation potential.

Having a closer look at the distribution of pixel values (see figure 19), scenario 2 was investigated as an example. Cooling capacity values are distributed in three main groups on the scale from 0 to 1. Most pixel values show relatively low values between 0,2 and 0,3, followed by another pixel group with the value 1 and a third one around the value of 0,7. The mean value of the distribution is not expressive.

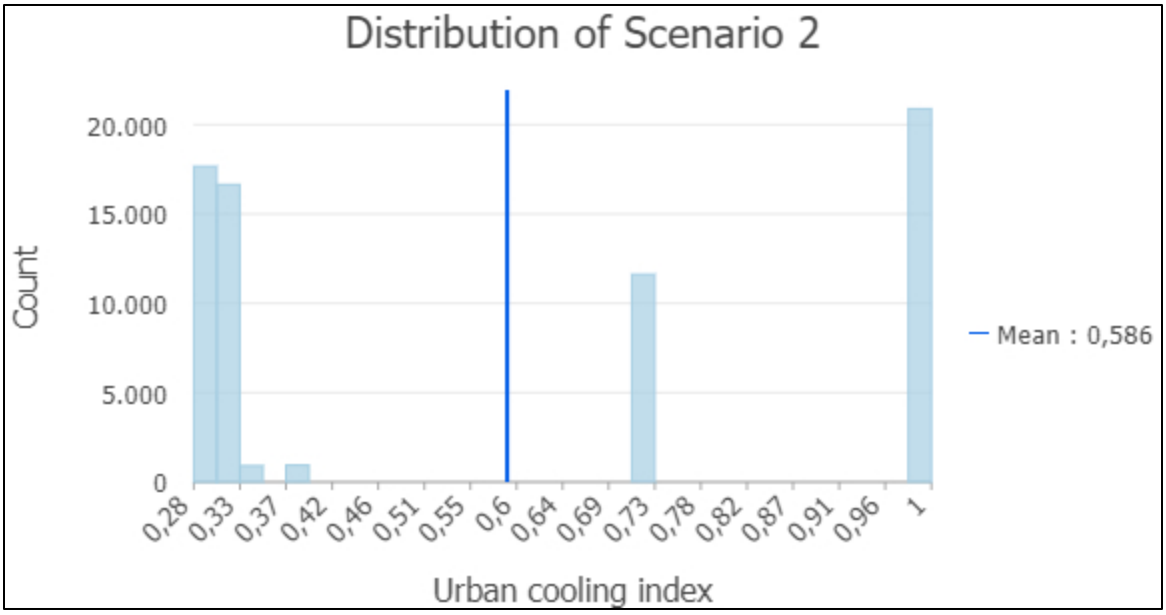

Figure 19: Distribution of pixel values of scenario 2

5.2.1 Parameter sensitivity

Since scenario 2 shows the cooling effect of urban green space in the most visible way, this scenario was chosen to test the sensitivity of several input parameters of the InVEST urban cooling model. As the model inputs can be modified very easily and the model runs rather quickly, numerous input parameters were changed.

It turned out, that changing the UHI magnitude by 2°C or the baseline air temperature by 3°C led to the exact same result. Bigger changes did not seem reasonable, as an UHI magnitude of 15°C for example, is a rather unlikely assumption for Vienna. The same applies for the baseline air temperature value. Modifying the air temperature maximum blending distance to either 200m or 1000m ended as well in the same output raster as with the initial 600m as InVEST urban cooling model input. Even though it was suggested in the model documentation that air temperature maximum blending distance may be used as a calibration parameter, it seems that the model is not sensitive at all to this parameter when applied on the 8th district of Vienna. Zero sensitiveness is seen for the earlier mentioned parameters UHI magnitude and baseline air temperature.

The indication of maximum cooling distance as model input was modified twofold. With an initial cooling distance of 450m, as suggested in the InVEST documentation, the parameter was both transformed to 300m and 600m for scenario 2. Figure 20 shows the urban cooling index output maps with modified input cooling distances. It can be observed that there are slight changes in these maps. However, only two classes seem to have changed, which are the ranges 0,2-0,3 and 0,3-0,4. By increasing the green area maximum cooling distance, the cooling capacity is increasing too. When reducing the maximum distance

parameter, the cooling capacity is also declining. This indicates a linear relationship between the green area maximum cooling distance and the cooling capacity.

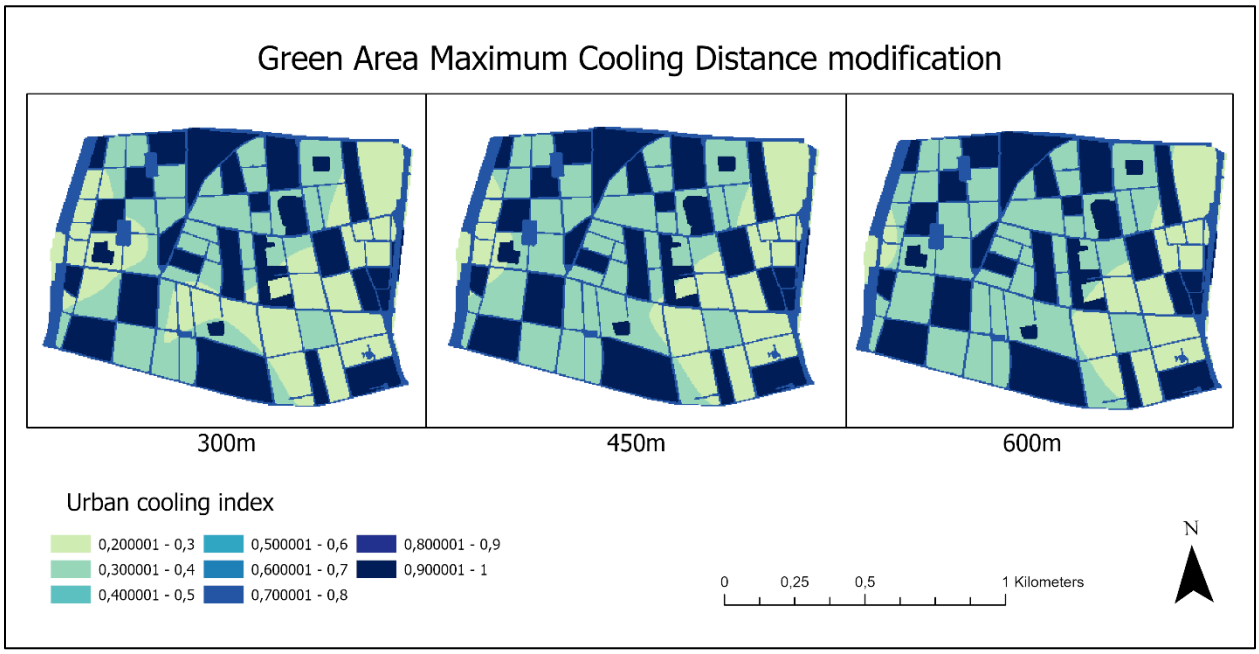

Figure 15: Green area maximum cooling distance modification outcomes

6 CONCLUSION

The main objective of this research was the evaluation of greening scenarios to mitigate urban heat islands during tropical nights. To conclude the findings of this research regarding the answering of the main objective, all research questions and its sub-questions will be examined in the following.

R1: Where are the urban heat islands of tropical nights in Vienna?

- Which thermal data are most suitable for nighttime UHI detection in Vienna?
- How can Vienna's detected urban heat islands be validated?
- How can the temperature hotspots be defined area wise in Vienna?

Nighttime urban heat islands are still an underrepresented research area due to the lack of nighttime temperature data. As ground measurements are generally hard to receive concerning the lack of a large crowd of measurements that allow the prediction of urban heat islands, thermal remote sensing data seem to be an easier accessible option. However, TIR data usually come with a coarser spatial resolution than spectral reflectance remote sensing data. Another challenge is the availability of nighttime data. ECOSTRESS, which launched in 2018, seems to fill this gap for certain areas around the globe. Due to its acquisition time of 3-5 days at different times during day and night and a moderate spatial resolution of 70m, these thermal data seem to be an excellent option for urban heat island purposes in general. Another benefit of ECOSTRESS are ready-to-use, fully calculated LST products, which allow for quicker UHI estimations.

From the validation analysis it can be concluded, that in situ temperature measurements tend to be a few degrees higher than land surface temperature derived from ECOSTRESS satellite data. Although, only 43 ground measurements were used to validate the ECOSTRESS thermal image, the absolute temperature difference was comparatively homogeneous for all measure points.

Moreover, validation results may differ when including more ground measurements for the designated urban area of interest. As in situ temperature data are relatively limited for this purpose, these data might be best collected directly in the field for the study of interest. For the scope of this thesis the expenditure of work was not commensurate to undertake this step, but it might be of interest for further research.

The evaluation of the land surface temperature map was decisive for the definition of a focus area. In fact, the idea was to target the scenario analysis on the most significant urban heat island area. Mean values for Vienna's districts and census areas were calculated that indicated three districts with a very high UHI effect during a tropical night. The limited green cover proportion of the 8th district

Josefstadt, which is the lowest within the whole city, made it an interesting choice for the scenario analysis with a lot of potential for change.

R2: How can greening measures to mitigate urban heat islands during tropical nights in Vienna be mapped in different scenarios?

- What is the current green share in the most significant tropical night's temperature hot spot in Vienna?
- How sensitive is the change of land cover to land surface temperature in Vienna?

The generation of greening scenarios was based on the actual land use/land cover of Josefstadt. The first sub-question was already examined in the process of the UHI hot spot definition, as three districts had equally high land surface temperature values. Therefore, Josefstadt's low green share rate served as crucial factor for this decision.

The second sub-question was targeted by use of the InVEST urban cooling model, which calculates an urban cooling index to evaluate the nighttime heat mitigation potential. By altering the spatial configuration of the urban land cover, model estimates can shed some light on the effects of green cover increase as instruments for urban heat mitigation. Three different scenarios were generated with 10%, 20% and 30% of green cover in Josefstadt. Despite being rather unrealistic modifications for urban planning in Vienna, the scenarios were created to emphasize the strong impact of urban green areas to nighttime urban heat reduction. With regard to the InVESt model outcomes, a strong correlation of urban green cover and cooling capacity was assumed, just by visually comparing land cover and the resulting cooling capacity.

Eventually, the urban cooling model was tested in reference to altered model inputs. It was found that the InVEST urban cooling model is not sensitive at all to the change of 3 parameters. Changes at the baseline air temperature, the UHI magnitude and the air temperature maximum blending distance had zero effect on the output data of the InVEST urban cooling model, when applying it on the 8th district of Vienna. It is possible though, that these model inputs may have a more significant impact on a larger study area or an area with different land use/land cover conditions. An observable effect regarding model sensitivity was detected by modifying the green area maximum cooling distance.

7 DISCUSSION

This section of the thesis illustrates the outcomes of the analysis in regards of further research, improvements and limitations.

Room for improvement can definitely be seen at the validation of the land surface temperature with in situ measurements. The inclusion of more ground measurements could enhance the reliability of the examined LST product. Due to lack of available in situ temperature measurements, the spatial extent of the validation was expanded. However, when focusing on urban heat islands, a higher number of reference data for the urban area would have been beneficial to support the use of LST as a proxy for urban heat.

In addition, when directly validating LST products of low spatial resolutions with in situ measurements, T-based methods tend to lack reliability. Since LST can vary by approximately 10K over a few meters in a heterogeneous surface, the assessment of the spatial representativeness of station observations at a given spatial resolution is inevitable to reliably validate remotely sensed LSTs (Yu et al., 2017). *"The term "spatial representativeness" refers to measurements of the degree to which ground-based observations can resolve the surrounding LST by extending to the satellite footprint."* (Yu et al., 2017; p.24). Even though there are several approaches to measure the spatial representativeness for station observations, these are mostly used for satellite-albedo, evapotranspiration, and leaf area index (LAI) products. Few assessments exist for station LST observations, which fortifies the uncertainty of the validation of LST products and hinders the application of in situ measurements (Yu et al., 2017). Accordingly, there is still room for improvement by taking into account the spatial representativeness of the ground measurements.

The image sharpening to receive more accurate land surface temperature data brought no result. The source of error could not be found either and requires further research. There may be an error in the calculated albedo due to shading. Using another algorithm to sharpen the ECOSTRESS image may be an alternative option. The used HUTS algorithm dates back to 2011 already. There may be better performing methods by now. Since ECOSTRESS LST have not been targeted much in literature yet, future studies could focus on image sharpening techniques for ECOSTRESS land surface temperature in urban areas.

The outputs of the InVEST urban cooling model confirmed the correlation of urban green spaces to heat mitigation. For the latter, an urban cooling index was calculated as proxy for the temperature reduction. The urban cooling model is a rather new instrument to predict cooling capacities in urban cities on basis of land cover changes. The model turned out to be an easily applicable tool for heat mitigation studies. It is well documented with additional sample data to adapt the model inputs. The required technical know-how is mainly based on GIS software for the preprocessing of data inputs. Despite being easy to handle, the gathering and

preprocessing of data to fit the model requirements, can be time-consuming. Nevertheless, the InVEST urban cooling model is definitely suitable for further UHI studies in order to support urban greening. Generally, it can be an instrument for urban planners to quantify the effects of vegetation in cities all over the world. For further studies, it may be of interest to investigate urban heat islands on a different scale. Whereas, within this thesis, the urban cooling model was only run for one district. There may be differences when running it for the whole city of Vienna. Since evapotranspiration was one of the model requirements, cities in other climatic zones may show diverse model outputs. Until now, there are not many publications with results of the urban cooling model, which leaves room for improvement for further studies.

8 LITERATURE

Akbari, H., Pomerantz, M., & Taha, H. (2001). Cool surfaces and shade trees to reduce energy use and improve air quality in urban areas. Solar energy, 70(3), 295-310.

Allegrini, J., Dorer, V., & Carmeliet, J. (2015). Influence of morphologies on the microclimate in urban neighbourhoods. Journal of Wind Engineering and Industrial Aerodynamics, 144, 108-117.

Allen, R. G., Pereira, L. S., Raes, D., & Smith, M. (1998). Crop evapotranspiration-Guidelines for computing crop water requirements-FAO Irrigation and drainage paper 56. Fao, Rome, 300(9), D05109.

Aram, F., García, E. H., Solgi, E., & Mansournia, S. (2019). Urban green space cooling effect in cities. Heliyon, 5(4), e01339.

ArcGIS StoryMaps (n.d.). Applying the InVEST Model. Retrieved on 24-05-2022 from: https://storymaps.arcgis.com/stories/55c6a84db09749fd98f00600e8a1fc3e

Arellano, B., & Roca, J. (2021). Remote sensing and night time urban heat island. ISPRS-International Archives of the Photogrammetry, Remote Sensing and Spatial Information Sciences, 43, 15-22.

Bahi, H., Mastouri, H., & Radoine, H. (2020). Review of methods for retrieving urban heat islands. Materials Today: Proceedings, 27, 3004-3009.

Balany, F., Ng, A. W., Muttil, N., Muthukumaran, S., & Wong, M. S. (2020). Green infrastructure as an urban heat island mitigation strategy—a review. Water, 12(12), 3577.

Barr, J., & Cohen, J. P. (2014). The floor area ratio gradient: New York City, 1890–2009. Regional Science and Urban Economics, 48, 110-119.

Benedict, M. A., & McMahon, E. T. (2012). Green infrastructure: linking landscapes and communities. Island press.

Boori, M. S., Balzter, H., Choudhary, K., Kovelskiy, V., & Vozenilek, V. (2015). A comparison of land surface temperature, derived from AMSR-2, Landsat and ASTER satellite data. Journal of Geography and Geology, 7(3), 61.

Bosch, M., Locatelli, M., Hamel, P., Remme, R. P., Jaligot, R., Chenal, J., & Joost, S. (2021). Evaluating urban greening scenarios for urban heat mitigation: a spatially explicit approach. Royal Society open science, 8(12), 202174.

Buyadi, S. N. A., Mohd, W. M. N. W., & Misni, A. (2013). Green spaces growth impact on the urban microclimate. Procedia-Social and Behavioral Sciences, 105, 547-557.

Chung, J., Lee, Y., Jang, W., Lee, S., & Kim, S. (2020). Correlation analysis between air temperature and MODIS land surface temperature and prediction of air temperature using TensorFlow long short-term memory for the period of occurrence of cold and heat waves. Remote Sensing, 12(19), 3231.

Copernicus Europe's eyes on Earth (2022). Demonstrating heat stress in European cities. Retrieved on 23-01-2022 from: https://climate.copernicus.eu/demonstrating-heat-stress-european-cities

Czachs, C., Reinwald, F., Damyanovic, D., Brandenburg, C., Gantner, B., Allex, B., ... & Liebl, U. (2013). Urban Heat Islands–Strategy Plan Vienna. In PLANNING TIMES–You better Keep Planning or You get in Deep Water, for the Cities they are A-Changin'. Proceedings of 18th International Conference on Urban Planning, Regional Development and Information Society (pp. 1037-1044). CORP–Compentence Center of Urban and Regional Planning.

Dominguez, A., Kleissl, J., Luvall, J. C., & Rickman, D. L. (2011). High-resolution urban thermal sharpener (HUTS). Remote Sensing of Environment, 115(7), 1772-1780.

Encyclopædia Britannica (2021). Vienna. Retrieved on 09-04-2021 from: https://www.britannica.com/place/Vienna/Evolution-of-the-modern-city

ESA (2000-2021). Land Surface Temperature. Retrieved on 05-03-2021 from: https://sentinel.esa.int/web/sentinel/userguides/sentinel3slstr/overview/geophysicalmeasurements/landsurfacetemperature#:~:text=Land%20Surface%20Temperature%20(LST)%20is,land%20derived%20from%20infrared%20radiation.&text=LST%20is%20not%20the%20same,in%20the%20daily%20weather%20report.

Fisher, J. B., Lee, B., Purdy, A. J., Halverson, G. H., Dohlen, M. B., Cawse-Nicholson, K., ... & Hook, S. (2020). ECOSTRESS: NASA's next generation mission to measure evapotranspiration from the international space station. *Water Resources Research*, *56*(4), e2019WR026058.

Hamel, P., Guerry, A. D., Polasky, S., Han, B., Douglass, J. A., Hamann, M., ... & Daily, G. C. (2021). Mapping the benefits of nature in cities with the InVEST software. npj Urban Sustainability, 1(1), 1-9.

Hashim, H., Abd Latif, Z., & Adnan, N. A. (2019). Urban vegetation classification with NDVI threshold value method with very high resolution (VHR) Pleiades imagery. The International Archives of Photogrammetry, Remote Sensing and Spatial Information Sciences, 42, 237-240.

Helloworlde (2022). What we do. Retrieved on 11-05-2022 from: http://helloworlde.com/

Hook, S. J. (2011). HyspIRI Level-2 Thermal Infrared (TIR) land surface temperature and emissivity algorithm theoretical basis document. Pasadena, CA: Jet Propulsion Laboratory, National Aeronautics and Space Administration, 2011.

Hulley (n.d.). Sharpen ECOSTRESS 70m land surface temperature to 30m resolution using Landsat 8 Surface Reflectance Data. Retrieved on 15-02-2022 from: https://view.officeapps.live.com/op/view.aspx?src=https%3A%2F%2Furbancanopy.s3-us-west-2.amazonaws.com%2FImageSharpening_Matlab.docx&wdOrigin=BROWSELINK

Hulley, G., Shivers, S., Wetherley, E., & Cudd, R. (2019). New ECOSTRESS and MODIS land surface temperature data reveal fine-scale heat vulnerability in cities: A case study for Los Angeles County, California. Remote Sensing, 11(18), 2136.

Huryna, H., Cohen, Y., Karnieli, A., Panov, N., Kustas, W. P., & Agam, N. (2019). Evaluation of TsHARP utility for thermal sharpening of Sentinel-3 satellite images using Sentinel-2 visual imagery. Remote Sensing, 11(19), 2304.

IBO – Österreichisches Institut für Baubiologie und -ökologie (2021). Wiener Tropennächte. Hitzeschutzmaßnahmen für den privaten Wohnbereich. Retrieved on 29-11-2021 from: https://www.ibo.at/wissensverbreitung/ibomagazin-online/ibo-magazin-artikel/data/wiener-tropennaechte

ISOCARP Institute (2021). Towards Climate Resilient Planning in Vienna: From Models to Climate Services. Retrieved on 09-04-2021 from: https://www.isocarp-institute.org/wp-content/uploads/2020/08/Review14_Towards-climate-resilient-Planning-in-Vienna.pdf

Kaplan, G., Avdan, U., & Avdan, Z. Y. (2018). Urban heat island analysis using the landsat 8 satellite data: A case study in Skopje, Macedonia. In Multidisciplinary Digital Publishing Institute Proceedings (Vol. 2, No. 7, p. 358).

Kong, F., Yin, H., James, P., Hutyra, L. R., & He, H. S. (2014). Effects of spatial pattern of greenspace on urban cooling in a large metropolitan area of eastern China. Landscape and Urban Planning, 128, 35-47.

Kuriata-Potasznik, A. B., & Szymczyk, S. (2016). Variability of the water availability in a river lake system–A case study of Lake Symsar. Journal of Water and Land Development.

Kyselý, J., Kalvová, J. & Květoň, V. Heat Waves in the South Moravian Region During the Period 1961-1995. Studia Geophysica et Geodaetica 44, 57–72 (2000). https://doi.org/10.1023/A:1022009924435

Li, Z. L., Wu, H., Wang, N., Qiu, S., Sobrino, J. A., Wan, Z., ... & Yan, G. (2013). Land surface emissivity retrieval from satellite data. International Journal of Remote Sensing, 34(9-10), 3084-3127.

Liu, X., & Shen, Y. (2018). Quantification of the impacts of climate change and human agricultural activities on oasis water requirements in an arid region: a case study of the Heihe River basin, China. Earth System Dynamics, 9(1), 211-225.

Liveup Homes (2020). What Is Floor Area Ratio (FAR) And Why It's Important. Retrieved on 14-05-2022 from: https://liveup.in/blogs/floor-area-ratio-far-explained/

Lowry, W. P. (1977). Empirical estimation of urban effects on climate: a problem analysis. Journal of Applied Meteorology, 16(2), 129–135.

Magistrat der Stadt Wien (2021). Wetter – Statistiken. Retrieved on 09-04-2021 from: https://www.wien.gv.at/statistik/wetter/

Nuruzzaman, M. (2015). Urban heat island: causes, effects and mitigation measures-a review. International Journal of Environmental Monitoring and Analysis, 3(2), 67-73.

Parastatidis, D., Mitraka, Z., Chrysoulakis, N., & Abrams, M. (2017). Online global land surface temperature estimation from Landsat. Remote sensing, 9(12), 1208.

Psenner, A. (2014). Das Wiener Gründerzeit-Parterre-Eine analytische Bestandsaufnahme. Pilotstudie-Abschlussbericht. Available online at https://publik. tuwien. ac. at/files/PubDat_240533. pdf.

Qiu, G. Y., LI, H. Y., Zhang, Q. T., Wan, C. H. E. N., Liang, X. J., & Li, X. Z. (2013). Effects of evapotranspiration on mitigation of urban temperature by vegetation and urban agriculture. Journal of Integrative Agriculture, 12(8), 1307-1315.

Rasul, A. (2018). Using Landsat 8 images along with Google Earth Engine for investigation the location of the crashed aircrafts.

Ring, Z., Damyanovic, D., & Reinwald, F. (2021). Green and open space factor Vienna: A steering and evaluation tool for urban green infrastructure. Urban Forestry & Urban Greening, 62, 127131.

Roca, J., & Arellano, B. (2020, May). Measuring night-time urban heat island. Still a pending issue. In EGU General Assembly Conference Abstracts (p. 19577).

Sahnoune, S., & Benhassine, N. (2017). Quantifying the impact of green-roofs on urban heat island mitigation. International Journal of Environmental Science and Development, 8(2), 116.

Schwarz, N., Lautenbach, S., & Seppelt, R. (2011). Exploring indicators for quantifying surface urban heat islands of European cities with MODIS land surface temperatures. Remote Sensing of Environment, 115(12), 3175-3186.

Sekertekin, A., & Bonafoni, S. (2020). Sensitivity Analysis and Validation of Daytime and Nighttime Land Surface Temperature Retrievals from Landsat 8 Using Different Algorithms and Emissivity Models. Remote Sensing, 12(17), 2776.

Shi, H., Xian, G., Auch, R., Gallo, K., & Zhou, Q. (2021). Urban Heat Island and its regional impacts using remotely sensed thermal data—A review of recent developments and methodology. Land, 10(8), 867.

Silvestri, M., Romaniello, V., Hook, S., Musacchio, M., Teggi, S., & Buongiorno, M. F. (2020). First comparisons of surface temperature estimations between ECOSTRESS, ASTER and Landsat 8 over Italian volcanic and geothermal areas. Remote Sensing, 12(1), 184.

Sobstyl, J. M., Emig, T., Qomi, M. A., Ulm, F. J., & Pellenq, R. M. (2018). Role of city texture in urban heat islands at nighttime. Physical review letters, 120(10), 108701.

Song, B., & Park, K. (2014). Validation of ASTER surface temperature data with in situ measurements to evaluate heat islands in complex urban areas. Advances in Meteorology, 2014.

Stadt Wien (2022). Baukörpermodell (LOD1.4) -Produktinformation. Retrieved on 03-05-2022 from: https://www.wien.gv.at/stadtentwicklung/stadtvermessung/geodaten/bkm/produkt.html

STATISTICS AUSTRIA (2021). Retrieved on 09-04-2021 from: file:///C:/Users/Schule/Downloads/bevoelkerungszahl_oesterreichs_stieg_auf_mehr_als_893_mio._zu_jahresbeginn.pdf

Taha, H. (1997). Urban climates and heat islands: albedo, evapotranspiration, and anthropogenic heat. Energy and buildings, 25(2), 99-103.

The Natural Capital Project, 2022. InVEST documentation. Retrieved on 03.05.2022 from: https://invest-userguide.readthedocs.io/en/latest/urban_cooling_model.html#data-needs

Tyrallová, L., Schernthanner, H., & Tamm, J. (2018) Fernerkundliche Detektion und Dauerbeobachtung urbaner Hitze-und Kälteinseln.

Vuckovic, M., Loibl, W., Tötzer, T., & Stollnberger, R. (2019). Potential of urban densification to mitigate the effects of heat island in Vienna, Austria. Environments, 6(7), 82.

White-Newsome, J. L., Brines, S. J., Brown, D. G., Dvonch, J. T., Gronlund, C. J., Zhang, K., ... & O'Neill, M. S. (2013). Validating satellite-derived land surface temperature with in situ measurements: A public health perspective. Environmental health perspectives, 121(8), 925-931.

Xue, J., Anderson, M. C., Gao, F., Hain, C., Sun, L., Yang, Y., ... & Schull, M. (2020). Sharpening ECOSTRESS and VIIRS land surface temperature using harmonized Landsat-Sentinel surface reflectances. Remote Sensing of Environment, 251, 112055.

Yamamoto, Y. (2006). Measures to mitigate urban heat islands. NISTEP Science & Technology Foresight Center.

Yu, W., Ma, M., Li, Z., Tan, J., & Wu, A. (2017). New scheme for validating remote-sensing land surface temperature products with station observations. Remote Sensing, 9(12), 1210.

Yue, W., Liu, X., Zhou, Y., & Liu, Y. (2019). Impacts of urban configuration on urban heat island: An empirical study in China mega-cities. Science of the Total Environment, 671, 1036-1046.

Zhou, D., Xiao, J., Bonafoni, S., Berger, C., Deilami, K., Zhou, Y., … Sobrino, J. (2018). Satellite Remote Sensing of Surface Urban Heat Islands: Progress, Challenges, and Perspectives. Remote Sensing, 11(1), 48. doi:10.3390/rs11010048

9 APPENDICES

9.1 APPENDIX A: MATLAB SCRIPT TO READ ECOSTRESS DATA, PREPROCESS IT AND WRITE IT TO A FILE

This script is primarily based on a publication of NASA's ECOSTRESS homepage, retrieved on 13-02-2022 from: https://ecostress.jpl.nasa.gov/faq

```
%read H5 file ECOSTRESS LST
ECO_LST1 =
hdf5read('ECOSTRESS_L2_LSTE_17018_010_20210707T040608_0601_01.h5','/SDS/LST','V71Dime
nsions',true);
ECO_LST1 = double(ECO_LST1).*0.02; %scale factor

%read quality control data, exclude poor quality pixels
QC =
hdf5read('ECOSTRESS_L2_LSTE_17018_010_20210707T040608_0601_01.h5','/SDS/QC','V71Dimen
sions',true);
test1 = bitget(QC,1);
test2 = bitget(QC,2);
QCtestgood = (test1==0 & test2==0);  %Best quality
ECO_LST1(~QCtestgood) = nan;

%Limits of study area
Lat_eco =
double(hdf5read('ECOSTRESS_L1B_GEO_17018_010_20210707T040608_0601_01.h5','/Geolocatio
n/latitude','V71Dimensions',true));
Lon_eco =
double(hdf5read('ECOSTRESS_L1B_GEO_17018_010_20210707T040608_0601_01.h5','/Geolocatio
n/longitude','V71Dimensions',true));
minlat = 48.1; maxlat = 48.35;
minlon = 16.15; maxlon = 16.61;
lats = minlat:0.0007:maxlat; lons = minlon:0.0007:maxlon;
[latg,long] = meshgrat(lats,lons);
latg = flipud(latg);
LSTgrid_eco = griddata(Lat_eco,Lon_eco,ECO_LST1,latg,long,'cubic');

%output data in a geotiff file
latlim = [min(latg(:)) max(latg(:))];
lonlim = [min(long(:)) max(long(:))];
rasterSize = size(latg);
R = georefcells(latlim,lonlim,rasterSize,'ColumnsStartFrom','north');
geotiffwrite('ECO2LST_neu.tif',LSTgrid_eco,R);
```

9.2 Appendix B: Matlab image sharpening script

The script is mainly based on a published script by Glynn Hulley (n.d.) and adjusted to meet the requirements of this thesis. The source script was accessed on 15-02-2022 at: https://view.officeapps.live.com/op/view.aspx?src=https%3A%2F%2Furbancanopy.s3-us-west-2.amazonaws.com%2FImageSharpening_Matlab.docx&wdOrigin=BROWSELINK

```
clc
clear all
%read each band from the Landsat image 30m
b2=imread("sr_viennac2.tif");
b4=imread("sr_viennac4.tif");
b5=imread("sr_viennac5.tif");
b6=imread("sr_viennac6.tif");
b7=imread("sr_viennac7.tif");

%NDVI
b4=double(b4);
b5=double(b5);
b4 = b4.*0.0001;
b5 = b5.*0.0001;
ndvi=(b5-b4)./(b5+b4);

%Albedo
b2=double(b2);
b6=double(b6);
b7=double(b7);
b2 = b2.*0.0001;
b6 = b6.*0.0001;
b7 = b7.*0.0001;
albedo = ((0.356*b2) + (0.130*b4) + (0.373*b5) + (0.085*b6) + (0.072*b7) -
0.0018)./1.016;

%read ECOSTRESS LST 70m
[ECO_LST,R] = geotiffread('ECO2LST_neu.tif');

% Get lat, lon limits
lonmin = R.LongitudeLimits(1);
lonmax = R.LongitudeLimits(2);
latmin = R.LatitudeLimits(1);
latmax = R.LatitudeLimits(2);

% Resize Landsat-8 30m data to ECOSTRESS 70m
res = size(ECO_LST);
NDVItir = imresize(ndvi,res);
Albedotir = imresize(albedo,res);

% Fitting coefficients that model LST using albedo and NDVI variables
xt = [318.5394 47.4863 -18.7976 -213.0017 23.6037 -148.3736 251.8148 -15.4255
373.1151 306.5941 -62.2609 -6.1342 -509.3209 -253.0092];

% low res LST fit for training
fitt1 = xt(1) + xt(2).*Albedotir + xt(3).*NDVItir + xt(4).*Albedotir.^2 +
xt(5).*NDVItir.^2 + xt(6).*NDVItir.*Albedotir + xt(7).*Albedotir.^3 +
xt(8).*NDVItir.^3 + xt(9).*NDVItir.*Albedotir.^2 +xt(10).*NDVItir.^2.*Albedotir +
```

```
xt(11).*Albedotir.^4 + xt(12).*NDVItir.^4 + xt(13).*NDVItir.*Albedotir.^3 +
xt(14).*NDVItir.^3.*Albedotir;

% diff between observed and low res fit
tdiff = ECO_LST-fitt1;

% Smoothing
% Building matrices that will compute running sums.  The left-matrix, eL, smooths
along the rows.  The right-matrix, eR, smooths along the columns.  You end up
replacing element "i" by the mean of a %(2*Nr+1)-by- (2*Nc+1) rectangle centered on
element "i".
matrixIn = tdiff;
N(1) = 2; N(2) = 2;  % Smooth over 2x2 pixels
[row,col] = size(matrixIn);
eL = spdiags(ones(row,2*N(1)+1),(-N(1):N(1)),row,row);
eR = spdiags(ones(col,2*N(2)+1),(-N(2):N(2)),col,col);

% Setting all "NaN" elements of "matrixIn" to zero so that these will not
% affect the summation.

A = isnan(matrixIn);
matrixIn(A) = 0;

% For each element, we have to count how many non-NaN elements went into
% the sums.  This is so we can divide by that number to get a mean.  We use
% the same matrices to do this (ie, "eL" and "eR").

nrmlize = eL*(~A)*eR;
nrmlize(A) = NaN;
matrixOut = eL*matrixIn*eR;
matrixOut = matrixOut./nrmlize;
tdiff_lr = matrixOut;

% high res sharpening LST fit
fitt2 = xt(1) + xt(2).*albedo + xt(3).*ndvi + xt(4).*albedo.^2 + xt(5).*ndvi.^2 +
xt(6).*ndvi.*albedo + xt(7).*albedo.^3 + xt(8).*ndvi.^3 + xt(9).*ndvi.*albedo.^2
+xt(10).*ndvi.^2.*albedo + xt(11).*albedo.^4 + xt(12).*ndvi.^4 +
xt(13).*ndvi.*albedo.^3 + xt(14).*ndvi.^3.*albedo;
tdiff_hr = imresize(tdiff_lr,size(fitt2),'nearest');

% Final 30m sharpened LST
LSTsharp = fitt2 + tdiff_hr;

%  Output the final sharpened LST at 30m resolution to a geotiff
latlim = [latmin latmax];
lonlim = [lonmin lonmax];
rasterSize = size(LSTsharp);
R1 = georefcells(latlim,lonlim,rasterSize,'ColumnsStartFrom','north');
geotiffwrite('ECO2LST_30m_2.tif',LSTsharp,R1);
```

9.3 Appendix C: LST map with exclusion of low-quality pixels

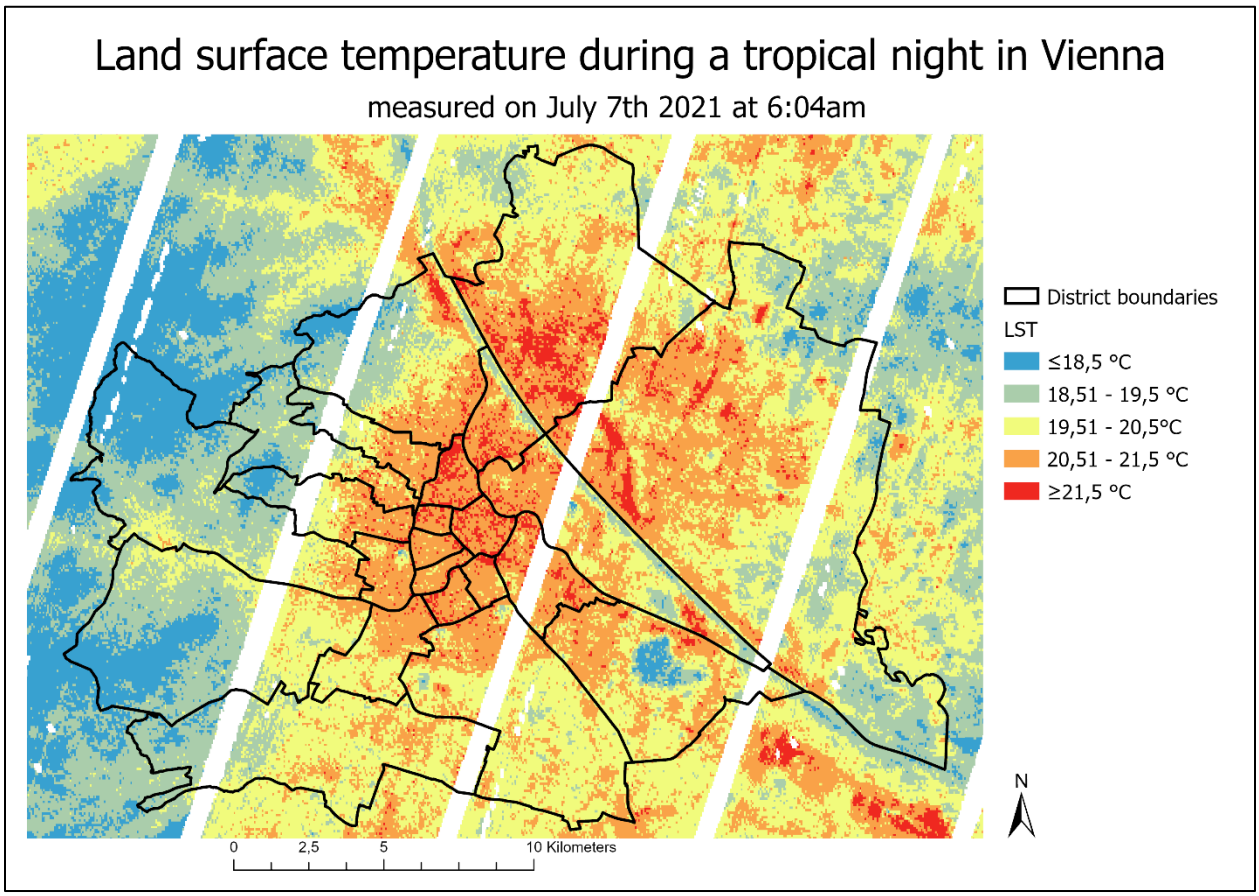

9.4 Appendix D: Sharpened 30m LST image

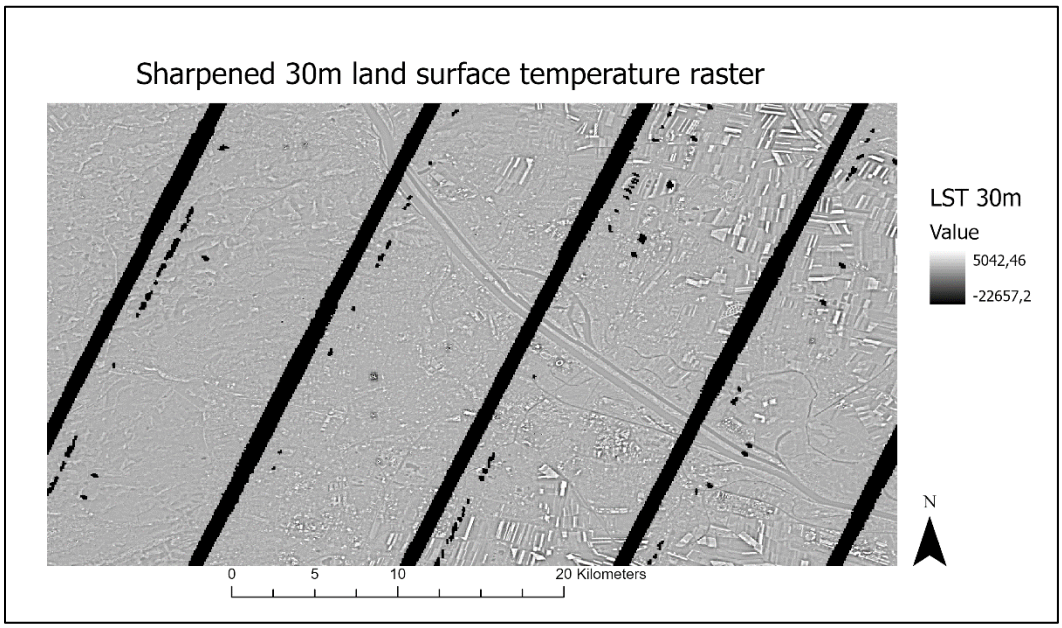

9.5 APPENDIX E: TABLE WITH VALIDATION OUTCOMES

Station number	Station measurements 2m T1 [°C]	Station measurements 5cm T2[°C]	LST mean Buffer 500m LST1 [°C]	Absolute difference T1 - LST1 [°C]	Absolute difference T2 - LST1 [°C]	LST mean Buffer 800m LST2 [°C]	Absolute difference T1 - LST2 [°C]	Absolute difference T2 - LST2 [°C]
5882	25,3	26,9	20,4	4,9	6,5	20,5	4,8	6,4
2117	21,2		17,0	4,2		17,2	4,0	
726	19,4	18,8	15,0	4,4	3,8	14,8	4,6	4,0
905	20,9	19,2	18,2	2,7	1,0	18,2	2,7	1,0
2207	22,1	26,7	18,6	3,5	8,1	18,4	3,7	8,3
2401	22,6	26,7	19,3	3,3	7,4	19,3	3,3	7,4
2430	23,3	23	19,2	4,1	3,8	19,2	4,1	3,8
2503	23,8	21,8	18,8	5,0	3,0	18,8	5,0	3,0
2601	24,1	24,9	19,0	5,1	5,9	18,9	5,2	6,0
4081	22,8	21,7	20,2	2,6	1,5	20,1	2,7	1,6
5609	21,0		19,1	1,9		19,0	2,0	
5625	19,4		16,7	2,7		17,0	2,4	
5701	22,9	17,8	17,5	5,4	0,3	17,6	5,3	0,2
5735	19,5	18,6	17,8	1,7	0,8	18,1	1,4	0,5
5802	20,8		18,4	2,4		18,5	2,3	
5805	23,4		19,8	3,6		19,8	3,6	
5904	24,0	21,2	20,8	3,2	0,4	20,8	3,2	0,4
5917	24,0	25,3	20,3	3,7	5,0	20,3	3,7	5,0
5990	24,1	26,3	20,2	3,9	6,1	20,4	3,7	5,9
7531	20,1		16,7	3,4		16,8	3,3	
7604	24,2	25,7	19,1	5,1	6,6	19,0	5,2	6,7
7610	20,6	17,3	16,8	3,8	0,5	16,6	4,0	0,7
7641	25,1		17,9	7,2		17,8	7,3	
10412	16,5		13,4	3,1		14,0	2,5	
10415	19,5	16,9	15,8	3,7	1,1	15,7	3,8	1,2
10510	22,6	19,1	15,9	6,7	3,2	15,8	6,8	3,3
10531	24,4		17,1	7,3		17,2	7,2	
10550	16,3		14,7	1,6		14,7	1,6	
3805	22,9	22	18,8	4,1	3,2	18,8	4,1	3,2
3811	22,4	25,3	17,7	4,7	7,6	17,6	4,8	7,7
4305	23,9		18,1	5,8		18,1	5,8	
4224	23,8	21,5	19,4	4,4	2,1	19,4	4,4	2,1
4030	22,9		19,7	3,2		19,7	3,2	
4115	23,4	21,4	19,8	3,6	1,6	19,9	3,5	1,5
4125	24,8	25,6	19,6	5,2	6,0	19,7	5,1	5,9
5820	23,9	32,6	20,0	3,9	12,6	19,9	4,0	12,7
5925	23,7		21,3	2,4		21,3	2,4	
5972	24,0	23,6	20,1	3,9	3,5	20,0	4,0	3,6
2116	21,6		15,1	6,5		15,3	6,3	
2415	20,2	20,1	17,9	2,3	2,2	18,0	2,2	2,1
7505	23,3	26,3	15,7	7,6	10,6	15,7	7,6	10,6
7710	25,8	24,1	19,0	6,8	5,1	18,9	6,9	5,2
5935	24,6	23,7	21,0	3,6	2,7	21,0	3,6	2,7
Mean	**22,4**	**22,9**	**18,3**	**4,1**	**4,2**	**18,3**	**4,1**	**4,2**